Geochemistry, Geophysics, Geosystems®

RESEARCH ARTICLE
10.1029/2021GC009847

Key Points:

- The Ojin Rise Seamounts are identified as intraplate hotspot track of the same mantle plume that formed the Shatsky Rise oceanic plateau
- Papanin Ridge formed by plume-ridge interaction and represents the northeastern continuation of the Shatsky plateau
- Linking an intraplate hotspot track to the Shatsky plateau confirms the involvement of a mantle plume for its formation

Supporting Information:

Supporting Information may be found in the online version of this article.

Correspondence to:

A. Dürkefälden,
aduerkefaelden@geomar.de

Citation:

Dürkefälden, A., Geldmacher, J., Portnyagin, M., Garbe-Schönberg, D., Werner, R., Müller, D., et al. (2021). Papanin Ridge and Ojin Rise Seamounts (Northwest Pacific): Dual hotspot tracks formed by the Shatsky plume. *Geochemistry, Geophysics, Geosystems*, *22*, e2021GC009847. https://doi.org/10.1029/2021GC009847

Received 19 APR 2021
Accepted 2 SEP 2021

Papanin Ridge and Ojin Rise Seamounts (Northwest Pacific): Dual Hotspot Tracks Formed by the Shatsky Plume

Antje Dürkefälden[1], Jörg Geldmacher[1], Maxim Portnyagin[1,2], Dieter Garbe-Schönberg[3], Reinhard Werner[1], Dietmar Müller[4], Folkmar Hauff[1], and Kaj Hoernle[1,3]

[1]GEOMAR Helmholtz Centre for Ocean Research Kiel, Kiel, Germany, [2]Vernadsky Institute of Geochemistry and Analytical Chemistry, Moscow, Russia, [3]Institute of Geosciences, Kiel University, Kiel, Germany, [4]EarthByte Group, School of Geosciences, The University of Sydney, Sydney, NSW, Australia

Abstract Although previous findings support an origin of the Shatsky Rise igneous plateau (Northwest Pacific) through interaction of a mantle plume with a mid-ocean ridge triple junction, the evidence for the involvement of a mantle plume is equivocal. The identification of an intraplate hotspot track emanating from the plateau could solve this controversy. Here we present major and trace element geochemical data from two different bathymetric features that emanate from the youngest end of Shatsky Rise: Papanin Ridge and the Ojin Rise Seamount province. Combining our results with plate tectonic reconstructions, we conclude that Papanin Ridge represents a hotspot track formed by plume-ridge interaction. Whereas the southwestern part was formed along the path of the retreating Pacific-Farallon-Izanagi triple junction, the northeastern part was built by preferential drainage into its Pacific-Farallon branch. In contrast, the Ojin Rise Seamounts formed as a true intraplate hotspot track of the Shatsky plume tail. Our wide-ranging study reveals systematic spatial geochemical variations, consistent with a lithospheric thickness control on magma composition derived from melting a heterogeneous plume source. The recognition of two hotspot tracks and in particular of the Ojin Rise Seamounts as an intraplate hotspot track that is directly linked to Shatsky plateau volcanism both in terms of geochemistry and plate tectonic reconstructions confirms the long-disputed involvement of a mantle plume for the formation of Shatsky Rise.

Plain Language Summary The origin of Shatsky Rise, a large igneous plateau in the NW Pacific, has long been debated. It could have either formed by shallow mantle melting due to its confirmed creation along a mid-ocean ridge or with additional contribution of deeper mantle material that upwelled as so-called mantle plume beneath the spreading ridge ("plume-ridge interaction"). The identification of an intraplate hotspot track emanating from Shatsky Rise and related to the plateau could answer this question. Here we present major and trace element geochemical data from lava samples dredged from two different structures that arise from the youngest end of the Shatsky Rise plateau: Papanin Ridge and the Ojin Rise Seamount province. By combining our results with plate tectonic reconstructions, we conclude that Papanin Ridge formed, like the main Shatsky Rise, by continued plume-ridge interaction. In contrast, the Ojin Rise Seamounts formed as a true intraplate hotspot track by the drift of the Pacific Plate over the stationary Shatsky hotspot (plume tail). The recognition of an intraplate hotspot track that is directly linked to the Shatsky plateau volcanism both in terms of geochemistry and plate tectonic reconstructions also confirms the involvement of a mantle plume for the formation of Shatsky Rise.

1. Introduction

The origin of vast oceanic volcanic plateaus is a subject of ongoing debate. According to the classical mantle plume model (e.g., Duncan & Richards, 1991; Richards et al., 1989), oceanic plateaus reflect the so-called plume head stage, when the uprising bulbous plume head impinges at the base of the lithosphere resulting in decompression melting and large-scale but relatively short-term lava outpourings on the overlying sea floor. During the following plume tail stage, an intraplate hotspot track (linear chain of ocean islands and seamounts) is formed while the plate moves above the much narrower plume tail. Alternatively, it was ar-

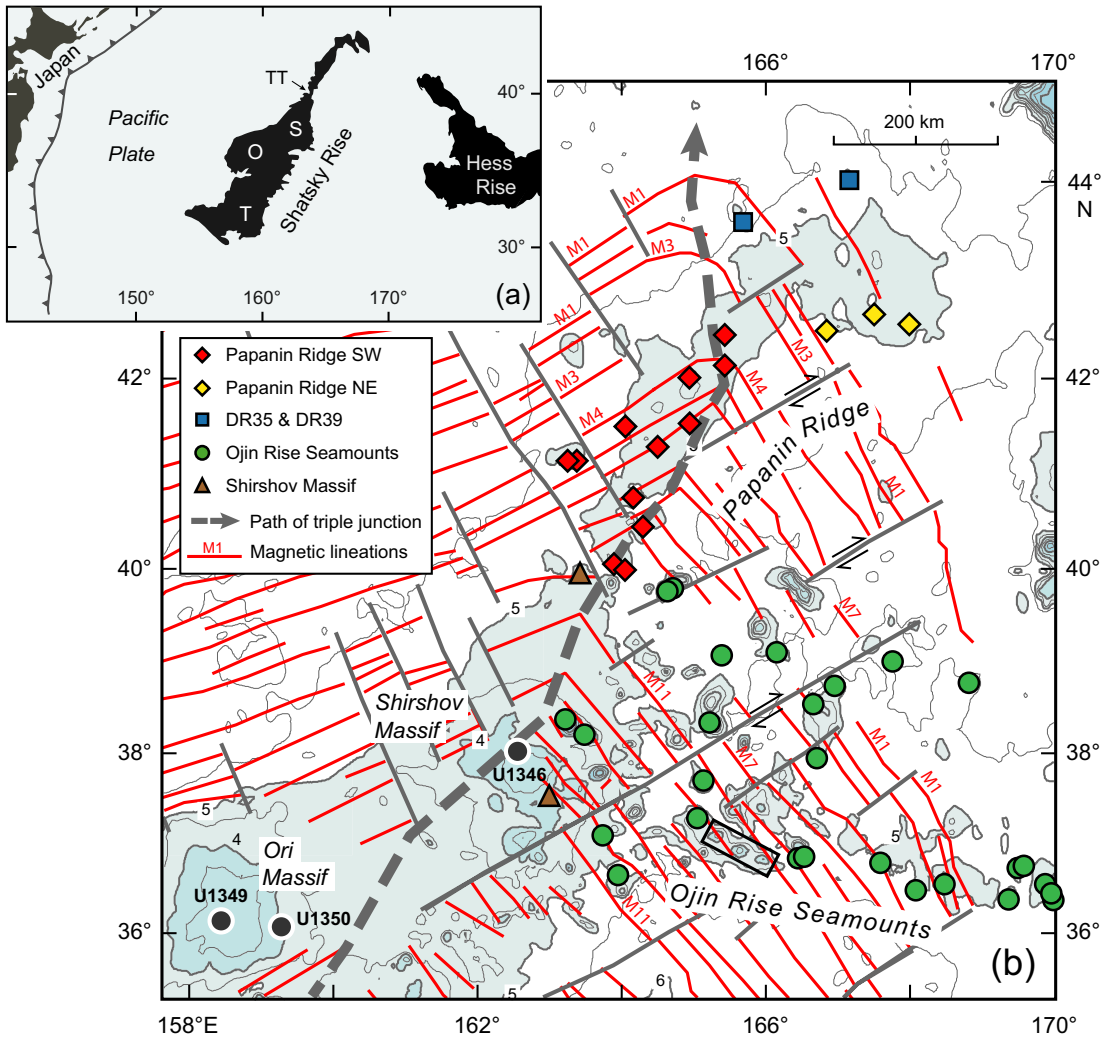

Figure 1. (a) Overview map of Shatsky Rise in the NW Pacific including the locations of the volcanic centers Tamu (T), Ori (O) and Shirshov (S) Massifs and Thompson Trough (TT) separating the main Shatsky plateau from Papanin Ridge. (b) Close-up map of Papanin Ridge emanating from the northern part of Shatsky Rise and the Ojin Rise Seamounts east of Shirshov Massif showing the sample locations of this study in different colors depending on their structural affiliation. Open box in the center of the Ojin Rise Seamounts encircles those investigated by Sano et al. (2020). Map modified after Sager et al. (2010) with light shaded areas above 5,000 m and magnetic anomaly lineations (red) and fracture zones (gray) after Nakanishi et al. (1999).

gued that oceanic plateaus could also form entirely by shallow mantle processes related to plate tectonics (e.g., Anderson, 2005; Foulger, 2007). More recently it has been suggested that the long-term interaction between plumes and mid-ocean ridges gives rise to oceanic plateaus (Jiang et al., 2021; Whittaker et al., 2015). The submarine Shatsky Rise, located in the northwest Pacific Ocean (Figure 1), might be a type example for this process, since it appears to have formed through interaction of a mantle plume with a triple junction (TJ) thus sharing both plume- and plate tectonic formation-related characteristics (see Sager et al., 2016 for overview). However, the involvement of a mantle plume is still controversially debated. A recent study by Sager et al. (2019) suggests that Tamu Massif, a part of Shatsky Rise, does not represent a shield volcano built by massive plume head activity as previously thought, but rather formed by voluminous spreading ridge volcanism. Identification of an intraplate hotspot track, emanating from the plateau as modeled by Wessel and Kroenke (2008) and Torsvik et al. (2019), would provide strong support for involvement of a plume. Two structures are directly adjacent to Shatsky Rise: Papanin Ridge and the Ojin Rise Seamount province. The major aim of this study is to investigate the post-plateau evolution of Shatsky Rise in order to test if these structures were formed as intraplate hotspot tracks by a proposed Shatsky mantle plume. Nearly 50 successful dredge hauls were conducted during R/V SONNE expedition SO265 in 2018 (Geldmacher

et al., 2018). Here we present new bathymetric and geochemical (major and trace element) data from volcanic rocks from Papanin Ridge and the Ojin Rise Seamounts and combine them with plate tectonic reconstructions. We conclude that Papanin Ridge is geochemically similar to the main Shatsky plateau and has formed by plume-ridge interaction, whereas the Ojin Rise Seamounts have compositions consistent with an intraplate formation and therefore could represent the long-sought main Shatsky Rise hotspot track. Thus, the Shatsky plume was involved in the formation of both structures, forming two hotspot tracks directly after formation of the Shatsky Rise plateau.

2. Geological Background and Previous Studies

Shatsky Rise is an oceanic plateau located ~1,500 km east of Japan in the northwest Pacific Ocean (Figure 1a). It covers an area of 5.3×10^5 km^2 (Zhang et al., 2016) making it the third largest oceanic plateau on Earth after the Ontong Java and Kerguelen plateaus. It has an estimated maximum crustal thickness of ~30 km based on seismic refraction surveys (Korenaga & Sager, 2012). Whereas other large oceanic plateaus formed during the Cretaceous normal superchron with no reversals of the Earth's magnetic field, the emplacement of Shatsky Rise took place in the Late Jurassic to Early Cretaceous during a period of frequent magnetic field reversals enabling the reconstruction of its original tectonic setting. Accordingly, the plateau formed by massive volcanism between magnetic chrons M21 and M11 (~145–133 Ma; Malinverno et al., 2012) along the path of a northeastward moving, fast-spreading TJ in a three-ridge configuration between the Pacific, Izanagi and Farallon plates (Nakanishi et al., 1999). The main part of Shatsky Rise consists of three huge volcanic edifices aligned in SW to NE direction (Tamu, Ori, and Shirshov Massifs), which rise >3,000 m above the surrounding seafloor (Figure 1). The emplacement of Tamu Massif marks the onset of Shatsky volcanism and Ar/Ar age dating reveals ages of ~145–143 Ma for its lavas (Geldmacher et al., 2014; Mahoney et al., 2005). These ages are in good agreement with magnetic anomalies M21–M19 of the underlying lithosphere, which correspond to ages of ~145–142 Ma, supporting the formation of Tamu Massif by interaction of a mantle plume with a TJ. Going toward the NE, the progressively younger volcanism of the Ori and Shirshov Massifs becomes less voluminous interpreted to reflect a waning plume head feeding the spreading center (Sager et al., 1999).

Shatsky Rise was drilled during IODP expedition 324 (Sager et al., 2010). Based on trace element enrichment, the recovered tholeiitic lavas were initially divided by Sano et al. (2012) into four geochemical magma types based on their Nb/Ti ratio, namely normal, low-Ti, high-Nb, and U1349 types. Since the normal and low-Ti types are genetically related and have identical isotopic compositions (Heydolph et al., 2014), they are now collectively considered as normal type (Sano et al., 2020). The normal type is the most abundant type and slightly enriched in incompatible elements compared with typical normal mid-ocean ridge basalt (N-MORB) compositions. The high-Nb type is more enriched in incompatible over less incompatible trace elements possessing signatures transitional between enriched (E-)MORB and ocean island basalt (OIB) compositions, whereas the U1349 type shows depleted compositions. Both the normal and high-Nb types could be associated with a mantle plume origin (moderately depleted and enriched plume components, respectively). The U1349 type, in contrast, most likely reflects entrainment of the local upper (MORB) mantle (Heydolph et al., 2014). Melting conditions for the normal type lavas have been calculated to be 15%–23% partial melting at >30 km (Husen et al., 2013; Sano et al., 2012) at source temperatures (TP) of 1,360–1,500°C (Kimura & Kawabata, 2015; Sano et al., 2012). Since these values are higher than those of MORB (but lower than inferred for the Ontong Java plateau magmas, e.g., Fitton & Godard, 2004), they point to the involvement of a mantle plume in Shatsky Rise formation.

The more than 500 km long and in its southern part ~100–150 km wide Papanin Ridge represents the northeastern continuation of the main plateau (Figure 1b) and is separated from Shirshov Massif by the WNW-ESE striking Thompson Trough (Figure 1a). Papanin Ridge is much less voluminous than the main plateau and relatively flat rising ~1,500–2,000 m above the abyssal plain. In contrast to Shatsky Rise with its focused edifices, the knolls on Papanin Ridge are relatively equally distributed and seldom form discrete summits. The ridge is underlain by magnetic anomalies M10 to M1 (~131–122 Ma) thus reflecting its maximum age. At ~42°30′N, 165°30′E after anomaly M4 (corresponding to CM5n), Papanin Ridge leaves the path of the TJ (Figure 1b) and bends to the ESE, where it broadens to ~200 km until it terminates at ~169°E. Before

expedition SO265, Papanin Ridge had never been sampled and therefore the composition of its rocks was unknown.

A number of models have been proposed to explain the formation of Papanin Ridge. It could be formed by the tail of a waning plume (Nakanishi et al., 1999; Sager et al., 1999) either still directly above the plume (on-axis), or by transfer of plume material toward the TJ (plume-ridge interaction). The northeast-trending Japanese and the southeast-trending Hawaiian magnetic lineations meet beneath the southwestern part of Papanin Ridge confirming that this part was still formed as the TJ continued moving northeastward (thick dashed gray line in Figure 1b). After magnetic chron M4, the ridge no longer lay on the path of the TJ. Thus, the NE bend of Papanin Ridge could have formed by intraplate volcanism above the tail of a mantle plume or by abandoned plume head material, acting as a stationary melting anomaly (Fletcher et al., 2020). If so, we would expect that lavas from both parts of Papanin Ridge would differ geochemically, for example, reflecting differences in melting depths beneath a TJ and a plate. Since the SE direction of the bend points toward the neighboring Hess Rise plateau, located just ~500 km away, a genetic link between the Shatsky and Hess Rise plateaus is widely considered (e.g., Bercovici & Mahoney, 1994; Fletcher et al., 2020; Kroenke & Sager, 1993; Nakanishi et al., 1999; Torsvik et al., 2019).

The Ojin Rise Seamounts are located east of Shirshov Massif with some seamounts situated on the margin of the massif itself and others extending over ~650 km to the ESE (Figure 1). The seamounts reside on crust that is somewhat thicker (~12 km) than normal oceanic crust (Shimizu et al., 2020) and ranges from M13 to M1 (~135-122 Ma). The seamount province comprises approximately 80 individual seamounts or seamount groups scattered over an area of ~220,000 km^2. It extends ~350 km in N-S direction in its central part and narrows to ~180 km at its easternmost end, eventually terminating at about 36°N, 170°E. Like the NE bend of Papanin Ridge, the province projects toward Hess Rise suggesting a possible link between these two large igneous plateaus.

Recent $^{40}Ar/^{39}Ar$ age dating from a seamount at 166°E (rectangular box in Figure 1b) revealed ages of 123.7–120.7 Ma (Sano et al., 2020) being 6–9 m.y. younger than the underlying seafloor (anomalies M8 to M9), indicating a formation in an intraplate setting and contemporaneous with the emplacement of the NE part of Papanin Ridge. Only a few Ojin Rise seamounts have been sampled and their lavas analyzed thus far. In contrast to the tholeiitic basalts from Shatsky Rise, they range from transitional/alkalibasaltic to trachybasaltic and basaltic trachyandesitic compositions (Sano et al., 2020; Tejada et al., 2016). Sano et al. (2020) distinguish between samples from the deeper, ridge-like base ("platform") and those from their smaller volcanic edifices ("cone") on top of the studied seamounts. Based on differences in petrography and geochemistry, the authors propose that the cones might represent intraplate seamounts formed by the Shatsky plume tail, whereas the NW-SE elongated platform might have formed slightly earlier at the Pacific-Farallon spreading center by plume-ridge interaction. Their interpretation is based on very few seamounts from a geographically restricted location near the center of the seamount province (rectangular box in Figure 1b). Until our study, the question if the Ojin Rise Seamount province (as a whole) or Papanin Ridge or at least its NE portion represent a true Shatsky intraplate hotspot track or, alternatively, if two hotspot tracks were formed by the same plume (a possibility demonstrated by e.g., Kumagai & Kurita, 1998) was not resolved.

3. Analytical Methods

In this study, geochemical data are presented for volcanic rocks obtained from 15 different dredge hauls along the entire length of Papanin Ridge including three sites on its NE bend (DR30, DR42, and DR45). Two distinct, isolated seamounts slightly north of the ridge (DR35 and DR39) were additionally mapped and sampled in order to test if these edifices can also be associated with Papanin Ridge. Two dredge hauls targeted slopes on Shirshov Massif and are therefore part of the main Shatsky Rise plateau (DR4 and DR75). From the Ojin Rise Seamounts, samples from 27 dredge hauls conducted at 23 different seamounts were analyzed. Locations of all sites from which samples were analyzed for this study are indicated in Figure 1b.

Established methods were used for the determination of major and trace element concentrations: whole rock compositions were measured by X-ray fluorescence spectrometry (XRF) and inductively coupled plasma mass spectrometry (ICP-MS), whereas glass compositions were determined by electron microprobe analysis (EMP) and laser ablation ICP-MS. Details about the methods are included in Text S1.

4. Results

4.1. Bathymetric Mapping

Multi-beam mapping of local areas of all sampled structures was carried out and revealed that Papanin Ridge consists of subcircular or elongated, often pancake-shaped summits and ridges, similar to shield volcanoes, which sometimes host small, possibly secondary, flat cones on top (Figure S1a). The larger edifices rise ~500–1,000 m above the toe of Papanin Ridge (roughly defined by the 5,000 m contour line). In contrast, the Ojin Rise Seamounts are generally morphologically more pronounced and show a large variety of shapes including pancake-shaped, conical, guyot-shaped and ridge-like (Figure S1b). The summits tower ~1,000–2,600 m above the surrounding abyssal plain. As also observed by Sano et al. (2020), some summits seem to be superimposed on a more widespread basement pedestal, which could also be a coalescing of neighboring seamounts. These structures often form NW-SE-oriented ridges parallel to the magnetic lineations (Figure 1). Some pancake-shaped or flat-topped seamounts show pronounced circular depressions (Figure S1c), a feature found on Papanin Ridge summits only at one location.

4.2. Petrography

All analyzed samples are volcanic rocks, which are moderately (10–40 vol.%) to highly (40–80 vol.%) altered based on the categorization of Sager et al. (2010) and mostly coated with a ferromanganese oxide crust of variable thickness (~1–30 mm). They contain vesicles ranging from 1 to 25 vol.% with a size of up to 10 mm, which are often filled with ferromanganese oxides or calcite.

Rocks from Shirshov Massif are aphyric to moderately porphyritic (≤5 vol.%) with plagioclase phenocrysts embedded in a fine-grained to microcrystalline groundmass consisting of plagioclase (~60–70 vol.%), pyroxene (~30–40 vol.%) and Fe-Ti oxide phases (~2–5 vol.%).

Papanin Ridge samples range from aphyric to highly plagioclase phyric (≤30 vol.% phenocrysts). At a few locations, moderately to highly olivine phyric (≤15 vol.%) rocks were also recovered with most olivines being completely replaced by iddingsite and saponite. The groundmass is fine-grained to microcrystalline and contains ~60–70 vol.% plagioclase, ~30–40 vol.% pyroxene and ~1–5 vol.% Fe-Ti oxide phases ± iddingsitized olivine (~1–2 vol.%). Samples from the two isolated seamounts north of Papanin Ridge (DR35 & DR39) are aphyric to sparsely porphyritic with plagioclase ± pyroxene phenocrysts (≤4 mm) in a fine-grained to microcrystalline groundmass similar to the Papanin Ridge samples but with ≤10 vol.% iddingsitized olivine.

Rocks recovered at the Ojin Rise Seamounts are aphyric to highly plagioclase phyric (≤30 vol.%) with plagioclase phenocrysts of up to 10 mm in size. Besides plagioclase, several samples from the western part of the Ojin Rise additionally contain 1–2 vol.% pyroxene phenocrysts, whereas rocks from DR14 at the northernmost sampled seamount from the rise contain ≤8 vol.% completely replaced olivine phenocrysts. The groundmass of the Ojin Rise samples is fine-grained to microcrystalline and consists of plagioclase (~60–70 vol.%), pyroxene (~30–40 vol.%) and Fe-Ti oxide phases (~1–5 vol.%) ± olivine (~1–2 vol.%) replaced by iddingsite and saponite.

4.3. Major and Trace Elements and the Effects of Alteration

Major and trace element contents for whole rock samples and glass chips are reported in Tables S2–S4. As expected for very old (early/mid Cretaceous) submarine volcanic rocks exposed to seawater over extended periods, the samples are moderately to heavily affected by seawater alteration resulting in a change of their bulk chemical composition. Besides coating by manganese crust and the filling of vesicles and cracks with secondary minerals, phosphatization is intense, a common feature of Pacific Ocean seafloor rocks of this age (e.g., Cullen & Burnett, 1986; Golowin et al., 2018; Hein, Koschinsky, et al., 2016). Due to the varyingly intense alteration of the samples with LOI values often exceeding 5 wt.%, major element results are only of limited use and thus a classification of the rocks based on the total alkali-silica diagram (TAS) is considered inappropriate. Likewise, the mobile trace elements Cs, Rb, and U (whose concentrations correlate with the LOI values of the samples) are not considered in this study, however, alteration shows a surprisingly minor effect on Sr concentrations. A common approach to mitigate the effects of alteration is to focus on minor and trace elements that are generally regarded as being immobile (and thus not sensitive for

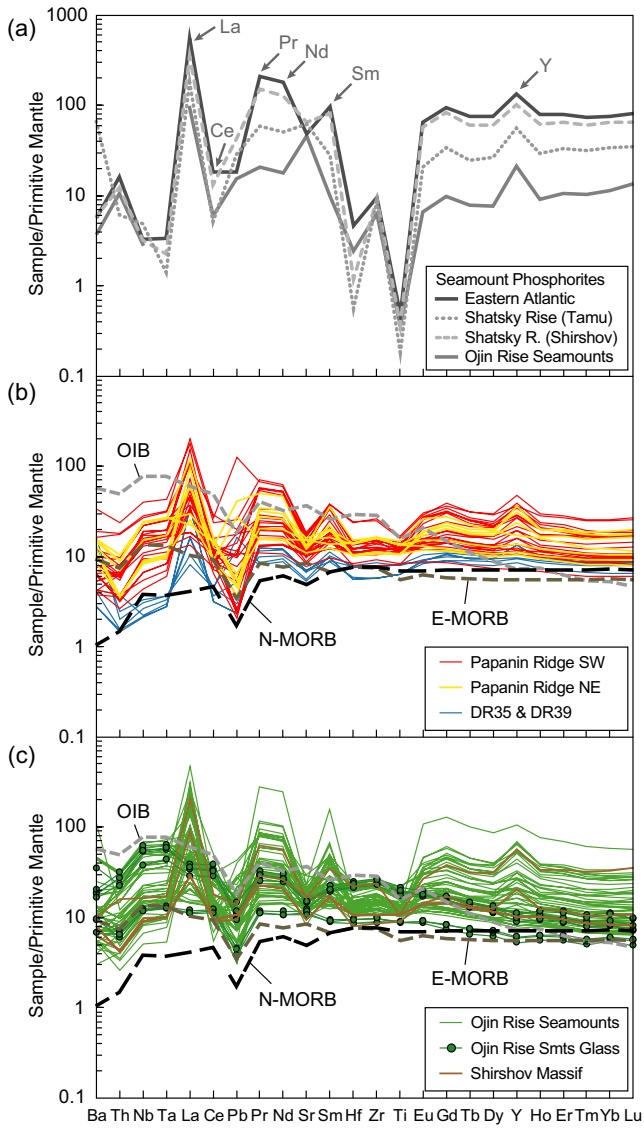

Figure 2. Multi-element diagrams normalized to primitive mantle values after Hofmann (1988) for (a) representative seamount phosphorites, (b) Papanin Ridge, and (c) Ojin Rise Seamounts and Shirshov Massif lavas analyzed for this study. A comparison with the patterns of seamount phosphorites from the Atlantic (Long et al., 2020) and Pacific Ocean (Hein, Koschinsky, et al., 2016; Sano et al., 2020) shows that the moderate to strong elevation of Y and the REEs (except Ce) displayed by many samples is caused by phosphatization of the rocks during seawater alteration processes. In contrast, the analyzed fresh glass samples from the Ojin Rise Seamounts preserved their original compositions. Papanin Ridge SW and NE samples show indistinguishable patterns, whereas the DR35 & DR39 samples resemble N-MORB. The Ojin Rise Seamounts lavas show stronger, OIB-like, enrichments of LREEs. Reference N-MORB, E-MORB, and OIB patterns are from Sun and McDonough (1989).

seawater alteration) including the high field strength elements (HFSEs) Nb, Ta, Hf, Zr, Y, Ti, and Th and the rare earth elements (REEs). As opposed to regular submarine alteration (i.e., transformation of interstitial glass and primary mineral phases to clay minerals and various uptake of ferromanganese, e.g., Staudigel et al., 1996), phosphatization, however, also affects the REEs and Y by incorporating these elements from seawater (e.g., Scopelliti et al., 2010). In addition to showing Ce depletion and enrichment in La, Pr, Nd, and Sm, the heavy REEs (HREEs) and Y are particularly enriched in seamount-covering phosphorites as demonstrated by representative phosphorites from Shatsky Rise (Hein, Koschinsky, et al., 2016), the Ojin Rise Seamounts (Sano et al., 2020) and the East Atlantic (Long et al., 2020), all shown in Figure 2a. Pervasive phosphatization of volcanic rocks exposed to seawater, often not detectable by the naked eye or even by thin section examination, can thus affect the REE and Y concentrations (also observed in submarine rocks from the Pacific by e.g., Finlayson et al. [2018] and Vanderkluysen et al. [2014]), which are normally a reliable indicator of certain magmatic processes, for example, depth or degree of melting. On multi-element diagrams (Figures 2b and 2c), most LREEs (e.g., La, Pr, Nd, and Sm), HREEs and Y of most analyzed samples show marked positive anomalies relative to the reference patterns for MORB and OIB, whereas Ce, in contrast, shows relative depletion. Relative Ce depletion is a known characteristic of (oxidized) seawater alteration (e.g., Elderfield & Greaves, 1982), which was already reported for dredged volcanic rocks from the main Shatsky plateau by Masuda and Nagasawa (1975).

In order to filter out samples that are significantly influenced by phosphatization, we consider the degree of relative enrichment of Y in combination with P_2O_5 content and the $(Tb/Yb)_N$ ratio (N = normalized to primitive mantle values after Hofmann [1988]; Figure S2). The Y anomaly indicates the degree of phosphatization and is expressed by Y*, which is calculated as $Y^* = 2Y_N/(Dy_N + Ho_N)$, analogous to the calculation of Ce* (Hein, Conrad, et al., 2016). The $(Tb/Yb)_N$ ratio depicts the enrichment of the HREEs (including Yb), since pervasive phosphatization results in generally high concentrations and often increasing elevation from Ho to Lu as most clearly demonstrated by the Ojin Rise Seamounts phosphorite (Figure 2a). We observe an onset of a positive correlation of Y* with P_2O_5 for samples with $Y^* > 1.1$ (open symbols in Figure S2a), which accords with an onset of negative correlation of $(Tb/Yb)_N$ at the same Y* threshold, whereas samples with $Y^* \leq 1.1$ do not show any correlation with $(Tb/Yb)_N$ (filled symbols in Figure S2b). Note that drill samples from the main Shatsky plateau, which are non- or only marginally altered, possess Y* of up to 1.2. Based on the above described criteria, we filtered out all samples with $Y^* \geq 1.1$ and henceforth only consider the remaining samples (always indicated by filled sample symbols in the following figures).

In contrast to the altered crystallized rock samples, the few fresh volcanic glass remnants found in lavas from four Ojin Rise Seamounts dredge sites reflect their original magmatic (liquid) compositions that have not been changed by seawater alteration and thus can be used without constraints. Individual samples from which both whole rock and glass are available were used for intra-sample compositional comparisons (Figure S3). The results confirm the effect of variable extents of phosphatization on the REE and Y contents, whereas the HFSEs and to some extent Pb do not show obvious phosphatization effects. Thus, whole rock data for these elements or for ratios of these elements can be used for the characterization of the magma source, as long as no phenocryst phase is

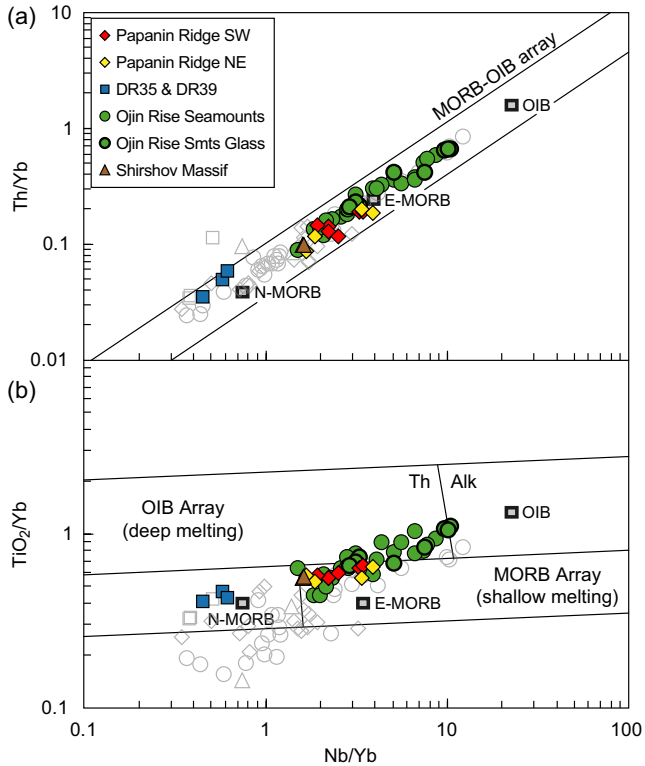

Figure 3. Nb/Yb versus (a) Th/Yb and (b) TiO_2/Yb diagrams after Pearce (2008). The Papanin Ridge lavas plot between N-MORB and E-MORB compositions and show no spatial compositional differences. Lavas from the Ojin Rise Seamounts also range between N- and E-MORB compositions, but a number of samples are more enriched trending toward OIB compositions. DR35 & DR39 lavas north of Papanin Ridge have compositions very similar to normal oceanic crust (N-MORB). Open symbols with gray frames indicate filtered data (see Figure S2).

present that could fractionate them. Volatile concentrations (Cl and S) in the glass samples, a description of the contents and their implication for source provenance and degassing can be found in Table S4 and Text S2.

4.4. Sample Characteristics and Classification

In order to detect possible geochemical differences pointing to distinct formation processes, we subdivide the Papanin Ridge lavas into a southwestern (Papanin Ridge SW) and a northeastern (Papanin Ridge NE) part by drawing the boundary at ~42°30′N, 165°30′E, where the ridge bends to the ESE (Figure 1).

The two sample groups, however, display overlapping compositions and are indistinguishable from each other in all compositional diagrams ranging between N-MORB and E-MORB signatures (Figure 3). The composition of the analyzed Shirshov Massif sample (DR4-1) is also very similar to those of the Papanin Ridge samples. In contrast, DR35 & DR39 lavas clearly possess N-MORB-like compositions and always plot as a distinct group (Figures 3, 4, and S4). The Ojin Rise Seamounts lavas range from more depleted (similar to Papanin Ridge) toward more enriched compositions ranging from E-MORB toward OIB type signatures. Note that even these (filtered) enriched samples do not show the strong depletion of the HREEs typical for OIBs indicative for melting primarily in the presence of garnet (retaining HREEs). The moderate HREE depletion of the Ojin Rise Seamounts lavas with $(Tb/Yb)_N \approx 1.2–1.8$, however, indicates that some garnet fractionation has played a role, in contrast to the group of Papanin Ridge samples, which cluster around $(Tb/Yb)_N = 1.3$ (Figure S2b). Whereas all Papanin Ridge, Shirshov Massif and DR35 & DR39 lavas fall within the MORB array in Figure 3b, the Ojin Rise Seamounts lavas overlap the Papanin Ridge samples and extend through the OIB tholeiitic to the boundary with OIB alkalic rocks, including all glass samples.

On the Nb/Ti versus Nb/Sc diagrams after Sano et al. (2012), lavas from both the SW and NE parts of Papanin Ridge mainly resemble the normal type with a few having higher Nb/Ti, slightly extending into the high-Nb type field (Figure S4). Again, no systematic difference between both parts of the ridge is observed. Lavas from the Ojin Rise Seamounts overlap with both the normal and high-Nb type fields. Sites DR35 & DR39 north of Papanin Ridge, in contrast, differ from all other compositions and are shifted to more depleted compositions and toward the U1349 type field.

5. Discussion

5.1. Origin of Papanin Ridge and Its Affiliation With Shatsky Rise

In general, Papanin Ridge lavas have compositions overlapping with the normal magma type of the Shatsky main plateau, which is the most abundant Shatsky magma type and also the only magma type found on Shirshov Massif thus far, the edifice located closest to Papanin Ridge. Since trace element variations reflect both mantle source and melting conditions, this observation suggests that Papanin Ridge most likely formed from the same source and under similar melting conditions and therefore in a similar tectonic regime as Shatsky Rise. The latter is also supported by the magnetic lineations, showing that Papanin Ridge formed along the path of the moving TJ up to ~42°30′N (before the SE bend; Figure 1). We therefore conclude that the SW part of Papanin Ridge developed by continued interaction of the presumed Shatsky plume with the spreading TJ, as proposed for Shirshov Massif/Shatsky Rise. The fact that Papanin Ridge shows much less volume and elevation than the main Shatsky plateau and forms a continuous ridge rather than discrete large massifs could either indicate that the plume source was already waning or that lesser amounts of plume material were drawn into the melting zone beneath the retreating TJ. Since the NE part of Papanin

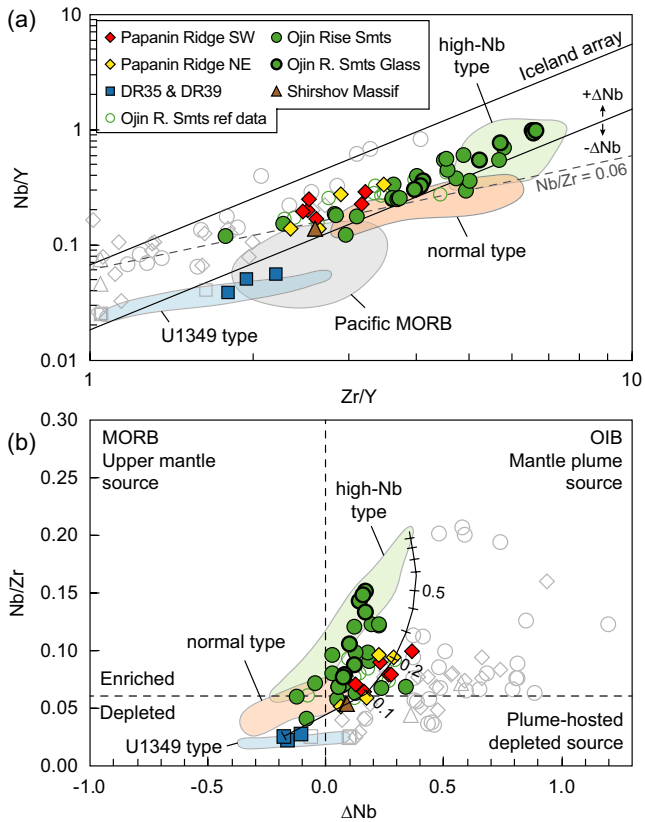

Figure 4. (a) Zr/Y versus Nb/Y diagram after Fitton et al. (1997) allowing the discrimination between plume and MORB mantle sources. Nearly all lavas from Shirshov Massif, Papanin Ridge and the Ojin Rise Seamounts from this study fall within the Iceland array indicating involvement of a plume source. DR35 & DR39 samples are an exception as most of them lie below the array and overlap with the Pacific MORB field as well as with the depleted U1349 type from the main plateau pointing to derivation from a MORB source. (b) ΔNb versus Nb/Zr diagram after Harpp and Weis (2020). This diagram allows the discrimination not only between enriched and depleted sources based on the boundary of Nb/Zr = 0.06 defined by Fitton et al. (2003) (see panel [a]), but also between a possible depleted plume source (positive ΔNb) and depleted upper mantle (negative ΔNb) which both could have Nb/Zr <0.06. The ΔNb value is based on the deviation from the lower bound of the Iceland array (Fitton et al., 1997; panel [a]). Included are fields for the different magma types found on the Shatsky Rise plateau (data sources are the same as in Figure S2) and Pacific MORB (from PetDB at http://www.earthchem.org/petdb). Endmembers for bulk mixing calculations in panel (b) are depleted sample DR35-1 (this study) and the most enriched Shatsky Rise high-Nb type drill sample from Ori Massif U1350A-17R-1, 43–47 cm with Nb/Zr = 0.203 and ΔNb = 0.353 (Sano et al., 2012). Open symbols with gray frames indicate filtered data.

Ridge was no longer formed at the TJ, we expected that the erupted lavas differ geochemically from the rest of the ridge caused by the so-called "lid effect" (e.g., Ellam, 1992; Haase, 1996; Niu et al., 2011). For instance, intraplate magmas erupting on thicker lithosphere away from a spreading center would have been produced at greater average depth/lesser degree of melting and should thus possess higher ratios of incompatible over less incompatible elements (e.g., increased Th/Yb) and/or possible greater depletion in HREEs (e.g., higher Tb/Yb). However, no such geochemical differences are observed (see Figures 3, S2, and S4) making an intraplate formation of this part of Papanin Ridge less likely. We therefore conclude that the NE part was also formed by plume-ridge interaction (drainage of plume material into a spreading center), albeit not at the retreating TJ (see Section 5.3).

To evaluate the role of the depleted upper mantle MORB source in Shatsky Rise and Papanin Ridge lava formation and a possible involvement of a depleted component intrinsic to the plume source, we use the the Zr/Y versus Nb/Y diagram after Fitton et al. (1997), which is often used for distinguishing between enriched plume mantle and depleted ambient upper mantle (Figure 4a). The "Iceland array" on this diagram defines a compositional range of plume-derived (within the array) and upper mantle (MORB)-derived (below the array) basalts in a geodynamic setting of assumed plume-ridge interaction such as Iceland or Shatsky Rise/Papanin Ridge. The deviation of individual samples from that array can be expressed by the ΔNb notation (see Figure 4). The normal and high-Nb type lavas from Shatsky Rise both lie on the lower bound of the array comprising samples with positive as well as negative ΔNb, but the high-Nb field shows considerably more overlap with the Iceland array (Figure 4a). This is consistent with enriched mantle plume material mixing with depleted upper mantle upwelling at a spreading ridge (TJ). Papanin Ridge lavas are somewhat different in that they exclusively plot within the Iceland array, as do almost all Ojin Rise Seamounts lavas, consistent with a plume involvement (see Section 5.2).

Combining ΔNb with Nb/Zr and using the boundary of Nb/Zr = 0.06 between enriched and depleted mantle sources as defined by Fitton et al. (2003) (dashed line in Figure 4a), it is further possible to distinguish a plume-hosted depleted source (Nb/Zr <0.06 and positive ΔNb values = lower right quadrant in Figure 4b) from a depleted non-plume (upper mantle) source (with Nb/Zr also <0.06 but negative ΔNb values = lower left quadrant) (Harpp & Weis, 2020). This discrimination is helpful, since incompatible-element and isotopically depleted lithologies can be intrinsic to mantle plumes (as suggested e.g., for the Galápagos and Manihiki plume sources; Golowin et al., 2018; Hoernle et al., 2000). The field of the normal type lavas from Shatsky Rise plots in the lower left quadrant but also slightly extends into the upper right quadrant consistent with depleted upper (N-MORB) mantle material mixed with some amount of enriched plume material. The high-Nb type field stretches from the upper boundary of the lower left quadrant far into the upper right quadrant indicating significantly less admixture of upper mantle material to the plume source. Note that both fields point toward distinct endmembers in the upper right quadrant indicating that the high-Nb type and the normal type represent different plume components that can independently mix with depleted upper (MORB) mantle, respectively.

The compositions of lavas from Papanin Ridge are shifted to slightly higher ΔNb compared with those from the main Shatsky plateau and form an array subparallel to the normal and high-Nb type fields. At first

glance, this distinct Papanin Ridge trend could reflect mixing between an enriched plume source (somewhere within the upper right quadrant) and an intrinsic depleted plume source (lower right quadrant). In contrast to all other Papanin Ridge samples, lavas from DR35 & DR39 dredged from two small isolated seamounts immediately north of NE bend of the ridge (Figure 1) show MORB-like depleted composition and overlap with the compositional field for U1349 type lavas from Shatsky Rise (Figure 4). The position of this field below the Iceland array (Figure 4a) and within the lower left quadrant in Figure 4b (Nb/Zr <0.06, ΔNb <0) is consistent with the assumption that the U1349 type lavas represent high degree melts of the local, upper mantle (Heydolph et al., 2014). Since the sampled DR35 & DR39 seamounts rise from the abyssal plain at a distance of ∼30–35 km from the outer edge of Papanin Ridge and are apparently not associated with the toe of the ridge, we conclude that these lavas represent Early Cretaceous oceanic crust formed immediately after the plume stopped interacting with the TJ (see Section 5.3). The composition of these lavas therefore represents the local upper mantle MORB source and can thus serve as potential depleted endmember for binary mixing models. Assuming that the most depleted DR35 & DR39 lava (sample DR35-1) most closely resembles the local upper mantle at the time of Papanin Ridge formation and that the most enriched high-Nb sample drilled at Shatsky Rise (sample U1350A-17R-1, 43–47; Sano et al., 2012) represents the enriched plume endmember, a binary mixing line would pass right through the Papanin Ridge data thereby explaining their shift toward slightly higher ΔNb values (Figure 4b) and arguing against an intrinsic depleted plume source endmember.

In summary, the compositions of Papanin Ridge lavas describe an overall mixing trend between a depleted (local upper mantle) and an enriched plume source analogous to the Shatsky Rise plateau lavas. This observation further confirms that although Papanin Ridge lavas have compositions similar to E-MORB in multi-element diagrams (Figure 2), an enriched (Shatsky plume) component is required for their magma genesis. However, neither the SW nor the NE part of Papanin Ridge represents an intraplate hotspot track. In the following, we therefore turn our attention to the Ojin Rise Seamounts.

5.2. Origin of the Ojin Rise Seamounts as Shatsky Intraplate Hotspot Track

Although several Ojin Rise Seamounts lavas compositionally overlap with Papanin Ridge and Shatsky Rise normal magma type lavas, the majority is distinctly more enriched and overlaps with the compositions of the enriched Shatsky Rise high-Nb type (Figures 4 and S4). Their OIB-like enrichment of incompatible over less incompatible elements and their stronger depletion of HREEs in comparison with the Papanin Ridge lava compositions indicate that these seamounts could indeed be formed in an intraplate setting beneath a lithospheric lid by overall lower degrees and higher pressures of partial melting. This would point to the seamount chain representing the hotspot track of the Shatsky plume during its plume tail stage. This is supported by the only available radiometric age determination from an Ojin Rise seamount located roughly in the center of the cluster (right summit in small box shown in Figure 1b), yielding an age of 121–124 Ma (Sano et al., 2020), which is ∼6–9 Ma younger than the magnetic lineation age of its underlying crust (M8-M9, ∼129–130 Ma using the time scale of Malinverno et al. [2012]).

However, the seamount lavas do not consistently show OIB-like compositions as would be expected for a typical hotspot track. Instead, they display a wide compositional range and span an array between depleted and enriched compositions pointing to generation beneath variably old/thin lithosphere. The seamount province extends from Shirshov Massif eastward to its termination at 36°N, 170°E with a strike of roughly WNW-ESE and thus almost perpendicular to the former Pacific-Farallon spreading center that ran NE of the seamounts with a NNW-SSE strike (see magnetic lineations in Figure 1). If the seamounts were not formed directly at the spreading ridge but on already existing oceanic crust at some distance from the spreading center, their lava chemistry should reflect a stronger lid effect (thicker lithosphere) in the NW and a weaker lid effect toward the SE due to progressively thinner lithosphere closer to the spreading center (e.g., Humphreys & Niu, 2009; Niu et al., 2011). The lid effect is particularly effective beneath young lithosphere, where lithospheric thicknesses and thus the depths of its base (where melting of upwelling material stops) describe a strongly convex curve (e.g., Parsons & Sclater, 1977). In fact, we observe that seamount lava chemistry becomes gradually depleted toward the east (Figure 5a). To correct for lateral offset of crust segments by fracture zones, we plot the degree of enrichment against the magnetic chron of the crust segment on which the respective seamounts were emplaced, serving as proxy for lithospheric age and thus

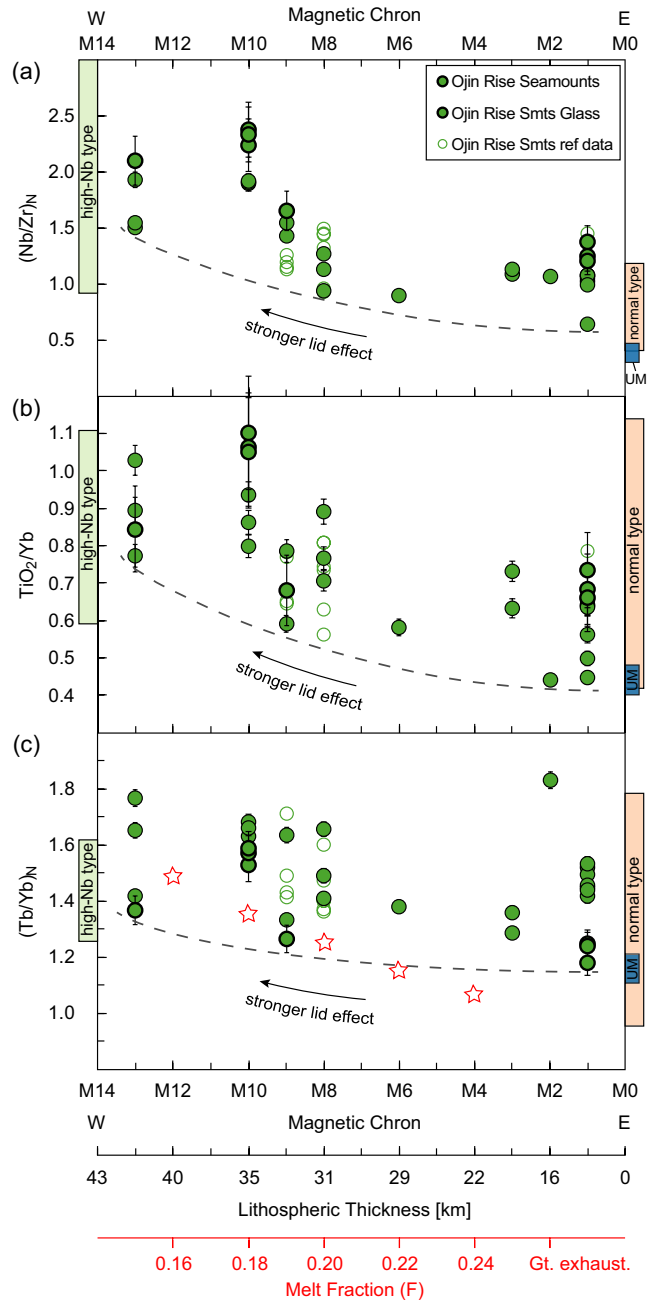

Figure 5. Mesozoic magnetic chrons (based on Nakanishi et al. [1999]) on which sampled Ojin Rise Seamounts are emplaced versus (a) $(Nb/Zr)_N$, (b) TiO_2/Yb, and (c) $(Tb/Yb)_N$ (normalized to primitive mantle values after Hofmann [1988]). The corresponding lithospheric thickness is approximated by assuming an eruption age at around chron M0 (see text for details) and the half-space lithosphere cooling model of $T = 11t^{1/2}$, where T is the lithospheric thickness in km and t is the age in Ma, which can be applied for lithosphere <~70 Ma (Humphreys & Niu, 2009). The lavas show a systematic spatial change in composition with lithospheric thickness, which becomes particularly clear if only the glass data are considered. The dashed line marks the lowest values best representing final melts at the upper end of their melting columns (see text). Also shown are the composition ranges for Shatsky Rise magma types after Sano et al. (2012) as orange and green fields and for DR35 & DR39 lavas (this study) as blue fields, representing the local upper (MORB) mantle composition (UM). HREE melt fraction modeling in (c) (red stars) was carried out using equations of Shaw (1970) for fractional melting and by assuming a source of Tb/Yb = 0.41 (equal to primitive mantle), basaltic K_D's from McKenzie and O'Nions (1991) and source mineralogy/initial melt proportions of: ol (0.55/0.14), opx (0.20/0.12), cpx (0.15/0.48), gt (0.05/0.21), and some already converted sp (0.05/0.05). Accordingly, the HREE depletion can be modeled by final melts having formed by approximately 18%–22% melting. Analytical errors are shown as bars.

thickness. Lesser depletion of the HREEs generally caused by a longer melting column allowing extended melting above the stability depths of garnet (and e.g., indicated by decreasing TiO_2/Yb or Tb/Yb) also seems to correlate with thinner lithosphere (lower numbers of magnetic chrons) (Figures 5b and 5c). All these correlations also hold and become particularly clear when only the available glass samples, which are not affected by alteration/phosphatization effects, are considered (Figure S5). Comparable systematics are reported from several near-ridge hotspot tracks, including Cobb, Easter and the early Hawaii-Emperor seamounts (Chadwick et al., 2014; Cheng et al., 1999; Regelous et al., 2003). For example, the Cobb Seamounts formed by the passage of the Pacific Plate (with variable lithospheric ages and thus thicknesses) over the Cobb hotspot since >33 Ma and show progressively depleted geochemical compositions as they become younger and erupted on thinner lithosphere closer to the Juan de Fuca Ridge (Chadwick et al., 2014). In the Ojin Rise Seamounts example, the Pacific-Farallon spreading center was not approaching, but the Pacific plate moved rapidly toward the NW, transporting progressively younger and thinner lithosphere over the stationary Shatsky plume (see discussion of plate tectonic reconstruction in Section 5.3).

Note that the trace element ratios from discrete samples from the same seamount or from different seamounts on equally thick lithosphere (same chron numbers) sometimes show a wide range. This is most likely caused by extraction of low-degree melts showing particular enrichment in incompatible elements by fractional melting followed by rapid eruption without effective pooling in shallow-level magma chambers. Therefore, only the lowest ratios of more to less incompatible-element ratios at any given site, which most closely reflect the highest degree of melting of an upwelling parcel of mantle material before hitting the base of the lithosphere, should be considered when assessing a correlation with such ratios (Figure 5). The convex systematics could reflect the exponential decrease of lithospheric thickness above the hotspot melting region. Single source melt modeling (Figure 5c) emphasizes the strong effect of residual garnet for the HREE depletion (such as Tb/Yb) but fails to reproduce the observed trends and reasonable degrees of melting. Instead, the systematic variation with lithospheric thickness can be best explained by a heterogeneous plume tail source consisting of more fertile, LREE-enriched material (namely the Shatsky high-Nb type) and more refractory, depleted lithologies (Shatsky normal type), which are also characterized by distinct HFSE ratios, in particular the different abundance of Nb (Figure 5a). The refractory, depleted material contributes to the melt composition in increasing proportions, when the melting column reaches shallower depths beneath young and thin lithosphere (higher degrees of melting). In contrast, the strongly LREE-enriched compositions reflect higher proportions of admixed low-degree (initial) melts of the enriched high-Nb type lithology at greater depths. An additional involvement of ambient upper (MORB) mantle cannot be ruled out, for example, dilution of enriched high-Nb type melt by depleted normal-type plume matrix plus additional minor admixture of ambient upper mantle, but these processes are difficult to distinguish solely based on major and trace element data.

The uncertainty of the exact eruption ages of the seamounts could also contribute to the range in geochemical composition observed for seamounts on equally thick lithosphere having the same chron. Unfortunately, the lack of regional radiometric age data from the Ojin Rise Seamounts currently does not allow us to accurately constrain the eruption ages for the respective sampled seamounts. We therefore revert to the often-confirmed model that the onset of intraplate hotspot volcanism of a former ridge-centered mantle plume roughly correlates with the cessation of large-scale drainage of plume material into the spreading center (e.g., Geldmacher et al., 2006; Sleep, 2002). At Shatsky Rise, this would correspond to chron <M1, when the formation of the NE part of Papanin Ridge came to an end (see Section 5.1). Accordingly, the Ojin Rise Seamounts should have erupted on lithosphere ranging from ~14 Ma in the west (135 Ma for M13 minus 121 Ma for M0) to <1Ma (M0) at the southeastern termination of the seamount group (Figure 1), corresponding to approximate (minimum) lithospheric thicknesses varying from ~41 to <11 km (see Figure 5 caption for applied equation). It is demonstrated by the only seamount for which a radiometric age is available that this relationship cannot be too erroneous (see Figure 1). This seamount sits on lithosphere of chron M9 (130 Ma) which should be, according to our assumption, ~9 to 8 Ma old at time M1–M0. Its $^{40}Ar/^{39}Ar$ age of 120.7–123.7 Ma (Sano et al., 2020) implies an actual lithospheric age of 9.3 to 6.3 Ma (at time of seamount formation) consistent with our estimate. By determining the effective elastic thickness (T_e) of the lithosphere beneath this central part of the seamount province, Shimizu et al. (2020) recently also concluded that this and the neighboring seamounts formed on young lithosphere near a spreading ridge, which we will further constrain in the next section.

5.3. Geodynamic Reconstruction

In the following, we attempt to reconstruct the formation of late stage Shatsky Rise and the Ojin Rise Seamounts based on our new geochemical findings and plate tectonic modeling by Wessel and Kroenke (2008; WK08-A), as implemented in Torsvik et al. (2019) and Müller et al. (2019), and discuss previously proposed models.

Reconstructing the motion of the early Pacific plate is challenging, since it was entirely surrounded by subduction zones before 83.5 Ma (e.g., Torsvik et al., 2019). In addition, several small ridge jumps and complex microplate tectonics during the formation of the Shatsky Rise plateau (e.g., Sager et al., 2019) make any constraints on the exact plume (center) location ambiguous. Since the youngest dated age from the Shatsky Rise plateau comes from a lava from Ori Massif (134 Ma; Heaton & Koppers, 2014), we have placed the plume center near Ori at this time as a starting position (Figure 6a) and then used the rotation parameters from Wessel and Kroenke (2008) for our reconstruction.

5.3.1. Formation of the SW Part of Papanin Ridge (Chrons M10 to M4, ~131–126 Ma)

As outlined in Section 5.1, the geochemical data are consistent with Papanin Ridge being formed at a spreading center by (Shatsky) plume-ridge interaction. As indicated by the magnetic lineations, the SW part of Papanin Ridge was formed along the path of the TJ either directly above the (waning) plume or by drainage of plume material into the northward-moving TJ (Figure 6a). In the latter case, the plume center would still be somewhere beneath northern Shatsky Rise at ~126 Ma, most likely at or near Shirshov Massif, consistent with the reconstruction model.

5.3.2. Formation of the NE Part of Papanin Ridge (Chrons M3 to M1, ~124–122 Ma)

At chron M4, the retreating TJ appears to have lost connection with the plume source consistent with increasing distance to a plume still centered at or near Shirshov Massif. Thus, the NE part (bend) of Papanin Ridge cannot have formed above the TJ. However, according to the underlying magnetic lineations, this part must have formed within ~3 Ma (M3–M1). The reconstruction (Figure 6b) reveals that the Pacific-Farallon spreading center, one of the three arms of the TJ, was still located in this area and was oriented in the same NW-SE direction as the bent part of Papanin Ridge. Due to the increased distance of the migrating TJ, plume material ceased to reach the TJ but was diverted into its closer NW-SE arm ("upside-down drainage" at the base of the lithosphere; e.g., Sleep, 1997).

Plume-ridge interaction is also observed at other hotspots such as Iceland, Galápagos and Kerguelen. Whereas the Iceland plume represents a ridge-centered hotspot (e.g., Wolfe et al., 1997), the Galápagos plume is presently located 100–200 km south of the Galápagos Spreading Center (e.g., Wilson & Hey, 1995). The Kerguelen Plateau and Broken Ridge were formed by long-term interaction of the Kerguelen plume with the Indian-Antarctic, Australian-Antarctic and Indian-Australian ridges, when the plume was located near-ridge (within 250 km) or temporarily beneath a ridge (Bredow & Steinberger, 2018; Jiang et al., 2021). Ongoing interaction with the Indian-Australian Ridge created the Ninetyeast Ridge and interaction with the Southeast Indian Ridge starting at ~40 Ma the Northern Kerguelen Plateau (e.g., Bredow & Steinberger, 2018). In both the Galápagos and Kerguelen systems, volcanic lineaments extend in a fan-shaped pattern between the hotspot and the ridge as a result of tensional stresses in the inside corner of a large-offset transform-ridge intersection associated with plume-ridge interaction (Harpp & Geist, 2002; Mittelstaedt & Ito, 2005; Mittelstaedt et al., 2012) rather than of channelized flow from the plume to the ridge as proposed by Morgan (1978) for the Wolf-Darwin Lineament at the Galápagos. Such lineaments, however, have not been detected at Papanin Ridge (nor the Ojin Rise) and probably could not develop due to the lack of nearby large-offset transforms along the Pacific-Farallon spreading center at the time of Papanin Ridge formation, and existing elongated structures run parallel instead of at right angle to the magnetic lineations and thus the spreading ridge.

At around 124 Ma (chron M2, corresponding to CM3n), the drift of the Pacific plate changed from a southwestern to western direction (Figure 6b). This change was accompanied by a significant slowdown of absolute plate motion (according to rotation parameters of Wessel and Kroenke [2008]) consistent with the assumed quasi-stationary position of the Shatsky plume center (plume stem) beneath the area of Shirshov Massif during M3–M1.

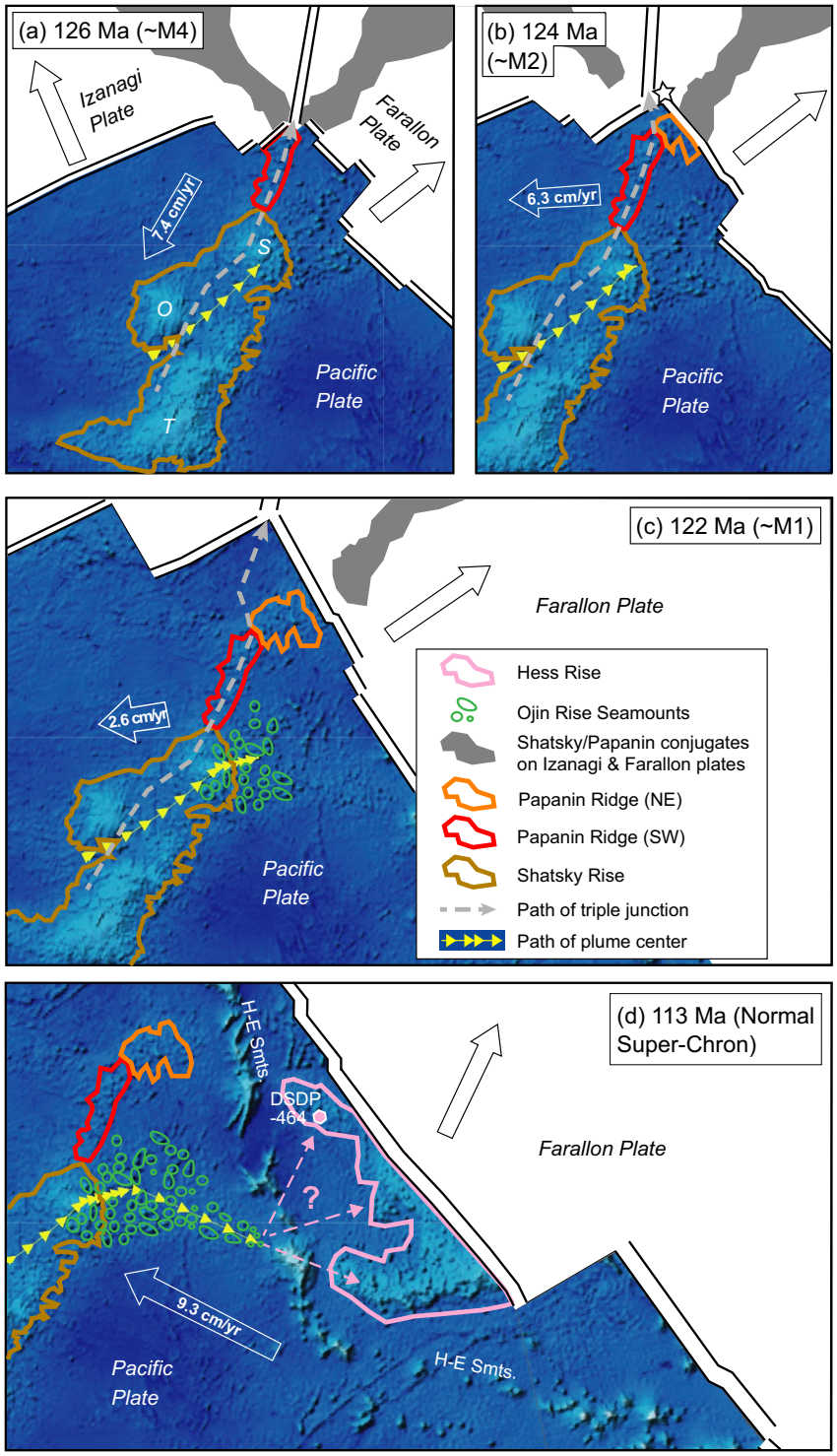
(a) 126 Ma (~M4)
Izanagi Plate
Farallon Plate
7.4 cm/yr
S
O
T
Pacific Plate
(b) 124 Ma (~M2)
6.3 cm/yr
Pacific Plate
(c) 122 Ma (~M1)
Farallon Plate
2.6 cm/yr
Pacific Plate
Hess Rise
Ojin Rise Seamounts
Shatsky/Papanin conjugates on Izanagi & Farallon plates
Papanin Ridge (NE)
Papanin Ridge (SW)
Shatsky Rise
Path of triple junction
Path of plume center
(d) 113 Ma (Normal Super-Chron)
H-E Smts.
DSDP -464
?
Farallon Plate
9.3 cm/yr
Pacific Plate
H-E Smts.

Figure 6.

More or less contemporaneously with formation of NE Papanin Ridge, the abyssal hills sampled at DR35 & DR39 also formed along the Pacific-Farallon spreading center, but further north and evidently beyond the influence of the inflowing plume material (white star in Figure 6b).

Recently, Fletcher et al. (2020) suggested a slightly different mechanism for the formation of the entire Papanin Ridge in that magmatic output was only derived from the plume head but not from the stem. They included numerical models suggesting that plume heads can be deformed, especially in the vicinity of spreading ridges or TJs. The increasing distance between the fixed plume stem (then generating the Ojin Rise Seamounts) and the TJ resulted in a disruption of plume material supply from the stem. Accordingly, Papanin Ridge was built up solely from melting of the detached, remaining shallow plume head material, which might provide an alternative explanation for the diminished magmatic output compared to the main plateau. The plume head then temporarily behaved as a stationary melting zone creating the NE bend of Papanin Ridge as intraplate "hotspot track." Our new geochemical data, showing no compositional differences between lavas from both parts of Papanin Ridge and thus indicating the same formation mechanism, do not support that view. In addition, Papanin Ridge lavas formed by a mixture of the enriched, high-Nb type plume material and local upper mantle beneath the respective spreading center and apparently without significant contribution from the normal type (Figure 4), which dominates the magmatic output of the mainly plume head-derived Shatsky Rise plateau. That relationship is also more consistent with the conventional drainage/mixing model.

With the cessation of fertile plume material/excess heat supply to the TJ, the formation of the conjugate plateaus at the two other corners of the TJ on the Izanagi and Farallon plates ceased as well and both conjugates eventually drifted away with their respective plates (see Figures 6a and 6b). Remnants of these plateaus can be found accreted to southwestern and northern Japan (Mikabu and Sorachi-Yezo ophiolites) and as subducted, seismically detectable, high-velocity body beneath central North America, respectively (e.g., Ichiyama et al., 2014; Liu et al., 2010).

5.3.3. Formation of the Ojin Rise Seamounts (Younger Than Chron M1, <122 Ma)

When large-scale drainage of plume material along the retreating spreading ridge ceased, the emplacement of the Ojin Rise Seamounts (cones) on the Pacific plate began in an intraplate setting consistent with the recent model of Sano et al. (2020). The initially very slow absolute westward Pacific plate motion during this time (~2.6 cm/yr) would allow a more widespread distribution of upwelling plume material beneath the lithosphere, which could explain why the seamount province forms such a scattered cluster at its NW end instead of a narrow hotspot track (Figure 6c). For instance, residual plume material would have time to pile up above the plume stem and thus deflect following upwelling material radially sideways (Hall & Kincaid, 2003). With the shift to a more pronounced NW direction and drastic acceleration of plate speed after 118 Ma (~9.3 cm/yr), the overall width of the province progressively narrowed down to a classical hotspot track toward its SE end reflected by the overall triangular shape of the seamount province (Figure 6d). Similarly, North Atlantic hotspots such as Madeira and the Canaries formed wide (~450 km) tracks at very slow average plate motions (1.2–1.6 cm/yr; Geldmacher et al., 2005), whereas South Atlantic hotspots beneath slightly faster moving lithosphere (2.0–3.1 cm/yr) generally produced narrower (~200–300 km) seamount chains (Homrighausen et al., 2020; Schwindrofska et al., 2016). Consequently, the fast movement rapidly

Figure 6. Plate tectonic reconstruction of Shatsky Rise and post-plateau Papanin Ridge and Ojin Rise Seamounts by using the GPlates software from Müller et al. (2018) with rotation parameters from Matthews et al. (2016) and the original Wessel and Kroenke (2008) poles (WK08-A). The motion path of the plume center (pointing in the opposite direction to plate motion) is shown with yellow arrows at 1 m.y. increments starting at 134 Ma near Ori Massif. (a) The SE part of Papanin Ridge (and respective conjugates on the Izanagi and Farallon plates) is constructed on the Pacific plate along the path of the TJ. At 126 Ma, the reconstructed center of the hotspot is located in the area of Shirshov Massif. Abbreviations for Shatsky Rise massifs: T, Tamu; O, Ori, S, Shirshov. (b) After the plume source lost connection with the TJ, the NE part of Papanin Ridge is formed by drainage of plume material into the Pacific-Farallon spreading center. The eruption site of the (MORB-like) DR35 & DR39 lavas is indicated by white star. (c) Formation of the scattered Ojin Rise Seamount province as true intraplate hotspot track above an extremely slowly moving (quasi-stationary) Pacific plate. (d) The shift to a more pronounced NW direction and drastic acceleration of plate speed after 118 Ma progressively narrowed down the overall width of the seamount province toward the SE. The cessation of the Ojin hotspot track at 170°E could reflect deflection and anew drainage of plume material into the Pacific-Farallon spreading center leading to formation of Hess Rise (dashed pink arrows). Note that the Hawaiian-Emperor Seamounts hotspot track (H-E Smts.) was formed much later and is not related to Shatsky plume activity.

brought the plume stem beneath progressively younger lithosphere consistent with the observed spatial geochemical gradient in the chemistry of the Ojin Rise Seamounts lavas (see Section 5.2).

Our reconstructed hotspot track (or Pacific plate motion path) differs from older models, but is very similar to the recently published path of Torsvik et al. (2019), who have used the same (original) rotation parameters from Wessel and Kroenke (2008; WK08-A) as applied for the reconstruction for this study. Likewise, the track connects Shatsky Rise via the Ojin Rise hotspot track with the Hess Rise plateau, which could have formed by a second plume head generated by the same Shatsky plume source in the lower mantle (an idea first proposed by Bercovici & Mahoney, 1994), or by excess volcanism when the Shatsky/Ojin plume tail was overridden by another major spreading center (e.g., Norton et al., 2007; Rea & Dixon, 1983). In any case, similar isotopic compositions of Shatsky and Hess Rise plateau lavas, although based on just two samples available from Hess Rise, and similar paleolatitude of the emplacement sites support the idea that both plateaus were fed by the same hotspot/mantle plume (Tejada et al., 2016; Torsvik et al., 2019). It is conceivable that the cessation of the Ojin Rise hotspot track at 170°E reflects beginning deflection and anew drainage of upwelling plume material into the nearby located Pacific-Farallon spreading center and thus the inception of Hess plateau formation (Figure 6d). It is striking that the earliest known age of Hess Rise lavas from a drill site at the eastern flank of the plateau (<113 Ma at DSDP Site 464; Vallier et al., 1983) coincides with the time when the reconstructed plume path was located beneath the SE end of the waning Ojin Rise hotspot track. It cannot, however, be ruled out that the Ojin Rise Seamount chain has continued further to the east but got subsequently buried by edifice volcanism and/or mass wasting products of the Emperor Seamounts, which crossed through this area between 50 and 56 m.y. (Sharp & Clague, 2006) due to the passage of the Pacific plate over the Hawaiian hotspot (Figure 6d).

6. Conclusions

1. Papanin Ridge formed by plume-ridge interaction. While the southwestern part was formed along the path of the retreating Pacific-Farallon-Izanagi triple junction, the northeastern part was exclusively built by drainage of plume material into its Pacific-Farallon branch. The lava chemistry of both parts can be explained though a mixture of an enriched Shatsky plume component (high-Nb type) with the upper mantle MORB source.
2. The Ojin Rise Seamounts formed as an intraplate hotspot track of the Shatsky plume (tail). Our area-wide survey reveals systematic spatial geochemical variations, consistent with lithospheric thickness control on magma composition when melting a heterogeneous plume source. The respective magma source endmembers are consistent with specific magma source types established for Shatsky Rise (high-Nb and normal types), further linking the Ojin Rise Seamounts with Shatsky Rise.
3. The recognition of the Ojin Rise Seamount province as intraplate hotspot track that is directly linked both in terms of geochemistry and by plate tectonic reconstruction models to the Shatsky plateau volcanism confirms the long-disputed involvement of a (deep) mantle plume for the formation of Shatsky Rise.
4. Our conclusions support the model that large oceanic igneous plateaus may generally be formed by interaction of a spreading center with a mantle plume and we show that two hotspot tracks can be formed by the same mantle plume, although only the Ojin Rise Seamounts represent a true intraplate hotspot track located above the plume.

Acknowledgments
The authors would like to thank Captain L. Mallon and his skillful crew on the R/V SONNE for their support on board. The authors also thank U. Westernströer for her analytical support and K. Pank, T. Lück, F. Hampel, and J. Lang for their assistance with sample preparation and appreciate fruitful discussions with M. Tejada. Many thanks to T. Sano, J. Konter, T. Morrow, and two anonymous reviewers for their constructive reviews that helped improve this manuscript and to J. Blichert-Toft for editorial handling. The authors acknowledge funding of the cruise and this study by the German Ministry of Education and Research (BMBF; 03G0265A to J. Geldmacher, K. Hoernle, and R. Werner) and thank GEOMAR Helmholtz Centre for Ocean Research Kiel for funding some of the analytical work.

Data Availability Statement

All data generated in this study are included in the Supporting Information S1 and can be found in the EarthChem database (https://doi.org/10.26022/IEDA/111976).

References

Anderson, D. L. (2005). Large igneous provinces, delamination, and fertile mantle. *Elements*, *1*(5), 271–275. https://doi.org/10.2113/gselements.1.5.271

Bercovici, D., & Mahoney, J. (1994). Double flood basalts and plume head separation at the 660-kilometer discontinuity. *Science*, *266*(5189), 1367–1369. https://doi.org/10.1126/science.266.5189.1367

Bredow, E., & Steinberger, B. (2018). Variable melt production rate of the Kerguelen hotspot due to long-term plume-ridge interaction. *Geophysical Research Letters*, *45*(1), 126–136. https://doi.org/10.1002/2017GL075822

Chadwick, J., Keller, R., Kamenov, G., Yogodzinski, G., & Lupton, J. (2014). The Cobb hot spot: HIMU-DMM mixing and melting controlled by a progressively thinning lithospheric lid. *Geochemistry, Geophysics, Geosystems*, *15*(8), 3107–3122. https://doi.org/10.1002/2014gc005334

Cheng, Q. C., Macdougall, J. D., & Zhu, P. (1999). Isotopic constraints on the Easter Seamount Chain source. *Contributions to Mineralogy and Petrology*, *135*(2), 225–233. https://doi.org/10.1007/s004100050508

Cullen, D. J., & Burnett, W. C. (1986). Phosphorite associations on seamounts in the tropical southwest Pacific Ocean. *Marine Geology*, *71*(3), 215–236. https://doi.org/10.1016/0025-3227(86)90071-X

Duncan, R. A., & Richards, M. A. (1991). Hotspots, mantle plumes, flood basalts, and true polar wander. *Reviews of Geophysics*, *29*(1), 31–50. https://doi.org/10.1029/90rg02372

Elderfield, H., & Greaves, M. J. (1982). The rare earth elements in seawater. *Nature*, *296*(5854), 214–219. https://doi.org/10.1038/296214a0

Ellam, R. M. (1992). Lithospheric thickness as a control on basalt geochemistry. *Geology*, *20*(2), 153–156. https://doi.org/10.1130/0091-7613(1992)020<0153:ltaaco>2.3.co;2

Finlayson, V. A., Konter, J. G., Konrad, K., Koppers, A. A. P., Jackson, M. G., & Rooney, T. O. (2018). Sr–Pb–Nd–Hf isotopes and $^{40}Ar/^{39}Ar$ ages reveal a Hawaii–Emperor-style bend in the Rurutu hotspot. *Earth and Planetary Science Letters*, *500*, 168–179. https://doi.org/10.1016/j.epsl.2018.08.020

Fitton, J. G., & Godard, M. (2004). Origin and evolution of magmas on the Ontong Java Plateau. *Geological Society, London, Special Publications*, *229*(1), 151–178. https://doi.org/10.1144/gsl.Sp.2004.229.01.10

Fitton, J. G., Saunders, A. D., Kempton, P. D., & Hardarson, B. S. (2003). Does depleted mantle form an intrinsic part of the Iceland plume? *Geochemistry, Geophysics, Geosystems*, *4*(3). https://doi.org/10.1029/2002GC000424

Fitton, J. G., Saunders, A. D., Norry, M. J., Hardarson, B. S., & Taylor, R. N. (1997). Thermal and chemical structure of the Iceland plume. *Earth and Planetary Science Letters*, *153*(3–4), 197–208. https://doi.org/10.1016/S0012-821X(97)00170-2

Fletcher, M., Wyman, D. A., & Zahirovic, S. (2020). Mantle plumes, triple junctions and transforms: A reinterpretation of Pacific Cretaceous – Tertiary LIPs and the Laramide connection. *Geoscience Frontiers*, *11*(4), 1133–1144. https://doi.org/10.1016/j.gsf.2019.09.003

Foulger, G. R. (2007). The "plate" model for the genesis of melting anomalies. In G. R. Foulger & D. M. Jurdy (Eds.), *Plates, Plumes and Planetary Processes: Geological Society of America Special Paper* (Vol. 430, pp. 1–28). https://doi.org/10.1130/2007.2430(01)

Geldmacher, J., Hauff, F., & Werner, R. (2018). *Cruise Report SO265 - SHATSKY EVOLUTION: Evolution of the Shatsky Rise Hotspot System, Yokohama (Japan) – Kaohsiung (Taiwan), 26.08. – 11.10.2018*. GEOMAR Report, N. Ser. 047 (p. 258).

Geldmacher, J., Hoernle, K., Bogaard, P. V. D., Duggen, S., & Werner, R. (2005). New $^{40}Ar/^{39}Ar$ age and geochemical data from seamounts in the Canary and Madeira volcanic provinces: Support for the mantle plume hypothesis. *Earth and Planetary Science Letters*, *237*(1), 85–101. https://doi.org/10.1016/j.epsl.2005.04.037

Geldmacher, J., Hoernle, K., Klügel, A., Bogaard, P. V. D., Wombacher, F., & Berning, B. (2006). Origin and geochemical evolution of the Madeira-Tore Rise (eastern North Atlantic). *Journal of Geophysical Research: Solid Earth*, *111*(B9). https://doi.org/10.1029/2005jb003931

Geldmacher, J., van den Bogaard, P., Heydolph, K., & Hoernle, K. (2014). The age of Earth's largest volcano: Tamu Massif on Shatsky Rise (northwest Pacific Ocean). *International Journal of Earth Sciences*, *103*(8), 2351–2357. https://doi.org/10.1007/s00531-014-1078-6

Golowin, R., Portnyagin, M., Hoernle, K., Hauff, F., Werner, R., & Garbe-Schönberg, D. (2018). Geochemistry of deep Manihiki Plateau crust: Implications for compositional diversity of large igneous provinces in the Western Pacific and their genetic link. *Chemical Geology*, *493*, 553–566. https://doi.org/10.1016/j.chemgeo.2018.07.016

Haase, K. M. (1996). The relationship between the age of the lithosphere and the composition of oceanic magmas: Constraints on partial melting, mantle sources and the thermal structure of the plates. *Earth and Planetary Science Letters*, *144*(1), 75–92. https://doi.org/10.1016/0012-821X(96)00145-8

Hall, P. S., & Kincaid, C. (2003). Melting, dehydration, and the dynamics of off-axis plume-ridge interaction. *Geochemistry, Geophysics, Geosystems*, *4*(9). https://doi.org/10.1029/2003GC000567

Harpp, K., & Geist, D. (2002). Wolf–Darwin lineament and plume–ridge interaction in northern Galápagos. *Geochemistry, Geophysics, Geosystems*, *3*(11), 1–19. https://doi.org/10.1029/2002GC000370

Harpp, K. S., & Weis, D. (2020). Insights into the origins and compositions of mantle plumes: A comparison of Galápagos and Hawai'i. *Geochemistry, Geophysics, Geosystems*, *21*(9), e2019GC008887. https://doi.org/10.1029/2019gc008887

Heaton, D., & Koppers, A. (2014). Constraining the rapid construction of Tamu Massif at an ~145 Myr old triple junction, Shatsky Rise. In *Goldschmidt Conference, Sacramento, 2014, abstract 948*.

Hein, J. R., Conrad, T., Mizell, K., Banakar, V. K., Frey, F. A., & Sager, W. W. (2016). Controls on ferromanganese crust composition and reconnaissance resource potential, Ninetyeast Ridge, Indian Ocean. *Deep Sea Research Part I: Oceanographic Research Papers*, *110*, 1–19. https://doi.org/10.1016/j.dsr.2015.11.006

Hein, J. R., Koschinsky, A., Mikesell, M., Mizell, K., Glenn, C. R., & Wood, R. (2016). Marine phosphorites as potential resources for heavy rare Earth elements and yttrium. *Minerals*, *6*(3), 88. https://doi.org/10.3390/min6030088

Heydolph, K., Murphy, D. T., Geldmacher, J., Romanova, I. V., Greene, A., Hoernle, K., et al. (2014). Plume versus plate origin for the Shatsky Rise oceanic plateau (NW Pacific): Insights from Nd, Pb and Hf isotopes. *Lithos*, *200–201*, 49–63. https://doi.org/10.1016/j.lithos.2014.03.031

Hoernle, K., Werner, R., Morgan, J. P., Garbe-Schönberg, D., Bryce, J., & Mrazek, J. (2000). Existence of complex spatial zonation in the Galápagos plume. *Geology*, *28*(5), 435–438. https://doi.org/10.1130/0091-7613(2000)028<0435:eocszi>2.3.co;2

Hofmann, A. W. (1988). Chemical differentiation of the Earth: The relationship between mantle, continental crust, and oceanic crust. *Earth and Planetary Science Letters*, *90*(3), 297–314. https://doi.org/10.1016/0012-821X(88)90132-X

Homrighausen, S., Hoernle, K., Zhou, H., Geldmacher, J., Wartho, J.-A., Hauff, F., et al. (2020). Paired EMI-HIMU hotspots in the South Atlantic—Starting plume heads trigger compositionally distinct secondary plumes? *Science Advances*, *6*(28), eaba0282. https://doi.org/10.1126/sciadv.aba0282

Humphreys, E. R., & Niu, Y. (2009). On the composition of ocean island basalts (OIB): The effects of lithospheric thickness variation and mantle metasomatism. *Lithos*, *112*(1), 118–136. https://doi.org/10.1016/j.lithos.2009.04.038

Husen, A., Almeev, R. R., Holtz, F., Koepke, J., Sano, T., & Mengel, K. (2013). Geothermobarometry of basaltic glasses from the Tamu Massif, Shatsky Rise oceanic plateau. *Geochemistry, Geophysics, Geosystems*, *14*(10), 3908–3928. https://doi.org/10.1002/ggge.20231

Ichiyama, Y., Ishiwatari, A., Kimura, J.-I., Senda, R., & Miyamoto, T. (2014). Jurassic plume-origin ophiolites in Japan: Accreted fragments of oceanic plateaus. *Contributions to Mineralogy and Petrology*, *168*(1), 1019. https://doi.org/10.1007/s00410-014-1019-1

Jiang, Q., Jourdan, F., Olierook, H. K. H., Merle, R. E., & Whittaker, J. M. (2021). Longest continuously erupting large igneous province driven by plume-ridge interaction. *Geology*, *49*(2), 206–210. https://doi.org/10.1130/g47850.1
Kimura, J.-I., & Kawabata, H. (2015). Ocean Basalt Simulator version 1 (OBS1): Trace element mass balance in adiabatic melting of a pyroxenite-bearing peridotite. *Geochemistry, Geophysics, Geosystems*, *16*(1), 267–300. https://doi.org/10.1002/2014gc005606
Korenaga, J., & Sager, W. W. (2012). Seismic tomography of Shatsky Rise by adaptive importance sampling. *Journal of Geophysical Research: Solid Earth*, *117*(B8). https://doi.org/10.1029/2012jb009248
Kroenke, L. W., & Sager, W. W. (1993). The formation of oceanic plateaus on the Pacific plate. *Eos*, *74*, 555.
Kumagai, I., & Kurita, K. (1998). Laboratory experiment on entrainment and life cycle of the starting plume. *Abstract of the 6th SEDI Symposium, Tours, France* (p. 183).
Liu, L., Gurnis, M., Seton, M., Saleeby, J., Müller, R. D., & Jackson, J. M. (2010). The role of oceanic plateau subduction in the Laramide orogeny. *Nature Geoscience*, *3*(5), 353–357. https://doi.org/10.1038/ngeo829
Long, X., Geldmacher, J., Hoernle, K., Hauff, F., Wartho, J.-A., & Garbe-Schönberg, C.-D. (2020). Origin of isolated seamounts in the Canary Basin (East Atlantic): The role of plume material in the origin of seamounts not associated with hotspot tracks. *Terra Nova*, *32*(5), 390–398. https://doi.org/10.1111/ter.12468
Mahoney, J. J., Duncan, R. A., Tejada, M. L. G., Sager, W. W., & Bralower, T. J. (2005). Jurassic-Cretaceous boundary age and mid-ocean-ridge–type mantle source for Shatsky Rise. *Geology*, *33*(3), 185–188. https://doi.org/10.1130/g21378.1
Malinverno, A., Hildebrandt, J., Tominaga, M., & Channell, J. E. T. (2012). M-sequence geomagnetic polarity time scale (MHTC12) that steadies global spreading rates and incorporates astrochronology constraints. *Journal of Geophysical Research: Solid Earth*, *117*(B6). https://doi.org/10.1029/2012jb009260
Masuda, A., & Nagasawa, S. (1975). Rocks with negative cerium anomalies, dredged from Shatsky Rise. *Geochemical Journal*, *9*(4), 227–233. https://doi.org/10.2343/geochemj.9.227
Matthews, K. J., Maloney, K. T., Zahirovic, S., Williams, S. E., Seton, M., & Müller, R. D. (2016). Global plate boundary evolution and kinematics since the late Paleozoic. *Global and Planetary Change*, *146*, 226–250. https://doi.org/10.1016/j.gloplacha.2016.10.002
McKenzie, D., & O'Nions, R. K. (1991). Partial melt distributions from inversion of rare Earth element concentrations. *Journal of Petrology*, *32*(5), 1021–1091. https://doi.org/10.1093/petrology/32.5.1021
Mittelstaedt, E., & Ito, G. (2005). Plume-ridge interaction, lithospheric stresses, and the origin of near-ridge volcanic lineaments. *Geochemistry, Geophysics, Geosystems*, *6*(6). https://doi.org/10.1029/2004GC000860
Mittelstaedt, E., Soule, S., Harpp, K., Fornari, D., McKee, C., Tivey, M., et al. (2012). Multiple expressions of plume-ridge interaction in the Galápagos: Volcanic lineaments and ridge jumps. *Geochemistry, Geophysics, Geosystems*, *13*(5). https://doi.org/10.1029/2012GC004093
Morgan, W. J. (1978). Rodriguez, Darwin, Amsterdam, A second type of Hotspot Island. *Journal of Geophysical Research: Solid Earth*, *83*(B11), 5355–5360. https://doi.org/10.1029/JB083iB11p05355
Müller, R. D., Cannon, J., Qin, X., Watson, R. J., Gurnis, M., Williams, S., et al. (2018). GPlates: Building a virtual Earth through deep time. *Geochemistry, Geophysics, Geosystems*, *19*(7), 2243–2261. https://doi.org/10.1029/2018gc007584
Müller, R. D., Zahirovic, S., Williams, S. E., Cannon, J., Seton, M., Bower, D. J., et al. (2019). A global plate model including lithospheric deformation along major rifts and orogens since the Triassic. *Tectonics*, *38*(6), 1884–1907. https://doi.org/10.1029/2018tc005462
Nakanishi, M., Sager, W. W., & Klaus, A. (1999). Magnetic lineations within Shatsky Rise, northwest Pacific Ocean: Implications for hot spot-triple junction interaction and oceanic plateau formation. *Journal of Geophysical Research: Solid Earth*, *104*(B4), 7539–7556. https://doi.org/10.1029/1999jb900002
Niu, Y., Wilson, M., Humphreys, E. R., & O'Hara, M. J. (2011). The origin of intra-plate ocean island basalts (OIB): The lid effect and its geodynamic implications. *Journal of Petrology*, *52*(7–8), 1443–1468. https://doi.org/10.1093/petrology/egr030
Norton, I. O., Foulger, G. R., & Jurdy, D. M. (2007). Speculations on Cretaceous tectonic history of the northwest Pacific and a tectonic origin for the Hawaii hotspot. In *Plates, Plumes and Planetary Processes* (Vol. 430). Geological Society of America. https://doi.org/10.1130/2007.2430(22)
Parsons, B., & Sclater, J. G. (1977). An analysis of the variation of ocean floor bathymetry and heat flow with age. *Journal of Geophysical Research*, *82*(5), 803–827. https://doi.org/10.1029/JB082i005p00803
Pearce, J. A. (2008). Geochemical fingerprinting of oceanic basalts with applications to ophiolite classification and the search for Archean oceanic crust. *Lithos*, *100*(1–4), 14–48. https://doi.org/10.1016/j.lithos.2007.06.016
Rea, D. K., & Dixon, J. M. (1983). Late Cretaceous and Paleogene tectonic evolution of the North Pacific Ocean. *Earth and Planetary Science Letters*, *65*(1), 145–166. https://doi.org/10.1016/0012-821X(83)90196-6
Regelous, M., Hofmann, A. W., Abouchami, W., & Galer, S. J. G. (2003). Geochemistry of Lavas from the Emperor Seamounts, and the Geochemical Evolution of Hawaiian Magmatism from 85 to 42 Ma. *Journal of Petrology*, *44*(1), 113–140. https://doi.org/10.1093/petrology/44.1.113
Richards, M. A., Duncan, R. A., & Courtillot, V. E. (1989). Flood basalts and hot-spot tracks: Plume heads and tails. *Science*, *246*(4926), 103–107. https://doi.org/10.1126/science.246.4926.103
Sager, W. W., Huang, Y., Tominaga, M., Greene, J. A., Nakanishi, M., & Zhang, J. (2019). Oceanic plateau formation by seafloor spreading implied by Tamu Massif magnetic anomalies. *Nature Geoscience*, *12*(8), 661–666. https://doi.org/10.1038/s41561-019-0390-y
Sager, W. W., Kim, J., Klaus, A., Nakanishi, M., & Khankishieva, L. M. (1999). Bathymetry of Shatsky Rise, northwest Pacific Ocean: Implications for ocean plateau development at a triple junction. *Journal of Geophysical Research: Solid Earth*, *104*(B4), 7557–7576. https://doi.org/10.1029/1998jb900009
Sager, W. W., Sano, T., & Geldmacher, J. (2010). Proceedings IODP (Vol. 324). Integrated Ocean Drilling Program Management International, Inc. https://doi.org/10.2204/iodp.proc.324.102.2010
Sager, W. W., Sano, T., & Geldmacher, J. (2016). Formation and evolution of Shatsky Rise oceanic plateau: Insights from IODP Expedition 324 and recent geophysical cruises. *Earth-Science Reviews*, *159*, 306–336. https://doi.org/10.1016/j.earscirev.2016.05.011
Sano, T., Hanyu, T., Tejada, M. L. G., Koppers, A. A. P., Shimizu, S., Miyazaki, T., et al. (2020). Two-stages of plume tail volcanism formed Ojin Rise Seamounts adjoining Shatsky Rise. *Lithos*, *372–373*, 105652. https://doi.org/10.1016/j.lithos.2020.105652
Sano, T., Shimizu, K., Ishikawa, A., Senda, R., Chang, Q., Kimura, J. I., et al. (2012). Variety and origin of magmas on Shatsky Rise, northwest Pacific Ocean. *Geochemistry, Geophysics, Geosystems*, *13*(8). https://doi.org/10.1029/2012GC004235
Schwindrofska, A., Hoernle, K., Hauff, F., van den Bogaard, P., Werner, R., & Garbe-Schönberg, D. (2016). Origin of enriched components in the South Atlantic: Evidence from 40 Ma geochemical zonation of the Discovery Seamounts. *Earth and Planetary Science Letters*, *441*, 167–177. https://doi.org/10.1016/j.epsl.2016.02.041

Scopelliti, G., Bellanca, A., Neri, R., & Sabatino, N. (2010). Phosphogenesis in the Bonarelli Level from northwestern Sicily, Italy: Petrographic evidence of microbial mediation and related REE behaviour. *Cretaceous Research*, *31*(2), 237–248. https://doi.org/10.1016/j.cretres.2009.11.004

Sharp, W. D., & Clague, D. A. (2006). 50-Ma initiation of Hawaiian-Emperor bend records major change in Pacific plate motion. *Science*, *313*(5791), 1281–1284. https://doi.org/10.1126/science.1128489

Shaw, D. M. (1970). Trace element fractionation during anatexis. *Geochimica et Cosmochimica Acta*, *34*(2), 237–243. https://doi.org/10.1016/0016-7037(70)90009-8

Shimizu, S., Nakanishi, M., & Sano, T. (2020). Near-ridge-axis volcanism affected by hotspot: Insights from effective elastic thickness and topography of the Ojin Rise Seamounts, east of Shatsky Rise in the northwest Pacific Ocean. *Earth, Planets and Space*, *72*(1), 11. https://doi.org/10.1186/s40623-020-1140-5

Sleep, N. H. (1997). Lateral flow and ponding of starting plume material. *Journal of Geophysical Research: Solid Earth*, *102*(B5), 10001–10012. https://doi.org/10.1029/97jb00551

Sleep, N. H. (2002). Ridge-crossing mantle plumes and gaps in tracks. *Geochemistry, Geophysics, Geosystems*, *3*(12), 1–33. https://doi.org/10.1029/2001GC000290

Staudigel, H., Plank, T., White, B., & Schmincke, H.-U. (1996). Geochemical fluxes during seafloor alteration of the basaltic upper oceanic crust: DSDP Sites 417 and 418. In *Subduction* (pp. 19–38).

Sun, S.-S., & McDonough, W. F. (1989). Chemical and isotopic systematics of oceanic basalts: Implications for mantle composition and processes. *Geological Society, London, Special Publications*, *42*(1), 313–345. https://doi.org/10.1144/gsl.sp.1989.042.01.19

Tejada, M. L. G., Geldmacher, J., Hauff, F., Heaton, D., Koppers, A. A. P., Garbe-Schönberg, D., et al. (2016). Geochemistry and age of Shatsky, Hess, and Ojin Rise seamounts: Implications for a connection between the Shatsky and Hess Rises. *Geochimica et Cosmochimica Acta*, *185*, 302–327. https://doi.org/10.1016/j.gca.2016.04.006

Torsvik, T. H., Steinberger, B., Shephard, G. E., Doubrovine, P. V., Gaina, C., Domeier, M., et al. (2019). Pacific-Panthalassic reconstructions: Overview, errata and the way forward. *Geochemistry, Geophysics, Geosystems*, *20*(7), 3659–3689. https://doi.org/10.1029/2019gc008402

Vallier, T. L., Dean, W. E., Rea, D. K., & Thiede, J. (1983). Geologic evolution of Hess Rise, central North Pacific Ocean. *GSA Bulletin*, *94*(11), 1289–1307. https://doi.org/10.1130/0016-7606(1983)94<1289:geohrc>2.0.co;2

Vanderkluysen, L., Mahoney, J. J., Koppers, A. A. P., Beier, C., Regelous, M., Gee, J. S., & Lonsdale, P. F. (2014). Louisville Seamount Chain: Petrogenetic processes and geochemical evolution of the mantle source. *Geochemistry, Geophysics, Geosystems*, *15*(6), 2380–2400. https://doi.org/10.1002/2014GC005288

Wessel, P., & Kroenke, L. W. (2008). Pacific absolute plate motion since 145 Ma: An assessment of the fixed hot spot hypothesis. *Journal of Geophysical Research: Solid Earth*, *113*(B6). https://doi.org/10.1029/2007jb005499

Whittaker, J. M., Afonso, J. C., Masterton, S., Muller, R. D., Wessel, P., Williams, S. E., & Seton, M. (2015). Long-term interaction between mid-ocean ridges and mantle plumes. *Nature Geoscience*, *8*(6), 479–483. https://doi.org/10.1038/ngeo2437

Wilson, D. S., & Hey, R. N. (1995). History of rift propagation and magnetization intensity for the Cocos-Nazca spreading Center. *Journal of Geophysical Research: Solid Earth*, *100*(B6), 10041–10056. https://doi.org/10.1029/95JB00762

Wolfe, C. J., Bjarnason, I. T., VanDecar, J. C., & Solomon, S. C. (1997). Seismic structure of the Iceland mantle plume. *Nature*, *385*(6613), 245–247. https://doi.org/10.1038/385245a0

Zhang, J., Sager, W. W., & Korenaga, J. (2016). The seismic Moho structure of Shatsky Rise oceanic plateau, northwest Pacific Ocean. *Earth and Planetary Science Letters*, *441*, 143–154. https://doi.org/10.1016/j.epsl.2016.02.042

References From the Supporting Information

Fricker, M. B., Kutscher, D., Aeschlimann, B., Frommer, J., Dietiker, R., Bettmer, J., & Günther, D. (2011). High spatial resolution trace element analysis by LA-ICP-MS using a novel ablation cell for multiple or large samples. *International Journal of Mass Spectrometry*, *307*(1), 39–45. https://doi.org/10.1016/j.ijms.2011.01.008

Garbe-Schönberg, C.-D. (1993). Simultaneous determination of thirty-seven trace elements in twenty-eight international rock standards by ICP-MS. *Geostandards Newsletter*, *17*(1), 81–97. https://doi.org/10.1111/j.1751-908X.1993.tb00122.x

Govindaraju, K. (1994). 1994 Compilation of working values and sample description for 383 geostandards. *Geostandards Newsletter*, *18*, 1–158. https://doi.org/10.1046/j.1365-2494.1998.53202081.x-i1

Griffin, W., Powell, W., Pearson, N., & O'Reilly, S. (2008). GLITTER: Data reduction software for laser ablation ICP-MS. *Laser Ablation-ICP-MS in the Earth Sciences*. Mineralogical Association of Canada Short Course Series (Vol. 40, pp. 204–207).

Hein, J. R., Koschinsky, A., Mikesell, M., Mizell, K., Glenn, C. R., & Wood, R. (2016). Marine phosphorites as potential resources for heavy rare Earth elements and yttrium. *Minerals*, *6*(3), 88. https://doi.org/10.3390/min6030088

Heydolph, K., Murphy, D. T., Geldmacher, J., Romanova, I. V., Greene, A., Hoernle, K., et al. (2014). Plume versus plate origin for the Shatsky Rise oceanic plateau (NW Pacific): Insights from Nd, Pb and Hf isotopes. *Lithos*, *200–201*, 49–63. https://doi.org/10.1016/j.lithos.2014.03.031

Hofmann, A. W. (1988). Chemical differentiation of the Earth: The relationship between mantle, continental crust, and oceanic crust. *Earth and Planetary Science Letters*, *90*(3), 297–314. https://doi.org/10.1016/0012-821X(88)90132-X

Husen, A., Almeev, R. R., Holtz, F., Koepke, J., Sano, T., & Mengel, K. (2013). Geothermobarometry of basaltic glasses from the Tamu Massif, Shatsky Rise oceanic plateau. *Geochemistry, Geophysics, Geosystems*, *14*(10), 3908–3928. https://doi.org/10.1002/ggge.20231

Jarosewich, E., Nelen, J. A., & Norberg, J. A. (1980). Reference samples for electron microprobe analysis. *Geostandards Newsletter*, *4*(1), 43–47. https://doi.org/10.1111/j.1751-908X.1980.tb00273.x

Jochum, K. P., Stoll, B., Herwig, K., Willbold, M., Hofmann, A. W., Amini, M., et al. (2006). MPI-DING reference glasses for in situ microanalysis: New reference values for element concentrations and isotope ratios. *Geochemistry, Geophysics, Geosystems*, *7*(2). https://doi.org/10.1029/2005GC001060

Jochum, K. P., Weis, U., Schwager, B., Stoll, B., Wilson, S. A., Haug, G. H., et al. (2016). Reference values following ISO guidelines for frequently requested rock reference materials. *Geostandards and Geoanalytical Research*, *40*(3), 333–350. https://doi.org/10.1111/j.1751-908X.2015.00392.x

Jochum, K. P., Weis, U., Stoll, B., Kuzmin, D., Yang, Q., Raczek, I., et al. (2011). Determination of reference values for NIST SRM 610–617 glasses following ISO guidelines. *Geostandards and Geoanalytical Research*, *35*(4), 397–429. https://doi.org/10.1111/j.1751-908X.2011.00120.x

Kendrick, M. A., Jackson, M. G., Kent, A. J. R., Hauri, E. H., Wallace, P. J., & Woodhead, J. (2014). Contrasting behaviours of CO_2, S, H_2O and halogens (F, Cl, Br, and I) in enriched-mantle melts from Pitcairn and Society seamounts. *Chemical Geology*, *370*, 69–81. https://doi.org/10.1016/j.chemgeo.2014.01.019

Kendrick, M. A., Kamenetsky, V. S., Phillips, D., & Honda, M. (2012). Halogen systematics (Cl, Br, I) in Mid-Ocean Ridge Basalts: A Macquarie Island case study. *Geochimica et Cosmochimica Acta*, *81*, 82–93. https://doi.org/10.1016/j.gca.2011.12.004

Long, X., Geldmacher, J., Hoernle, K., Hauff, F., Wartho, J.-A., & Garbe-Schönberg, C.-D. (2020). Origin of isolated seamounts in the Canary Basin (East Atlantic): The role of plume material in the origin of seamounts not associated with hotspot tracks. *Terra Nova*, *32*(5), 390–398. https://doi.org/10.1111/ter.12468

Mahoney, J. J., Duncan, R. A., Tejada, M. L. G., Sager, W. W., & Bralower, T. J. (2005). Jurassic-Cretaceous boundary age and mid-ocean-ridge–type mantle source for Shatsky Rise. *Geology*, *33*(3), 185–188. https://doi.org/10.1130/g21378.1

McCarron, A. P., Bigg, G. R., Brooks, H., Leng, M. J., Marshall, J. D., Ponomareva, V., et al. (2021). Northwest Pacific ice-rafted debris at 38°N reveals episodic ice-sheet change in late Quaternary Northeast Siberia. *Earth and Planetary Science Letters*, *553*, 116650. https://doi.org/10.1016/j.epsl.2020.116650

Michael, P. J., & Schilling, J.-G. (1989). Chlorine in mid-ocean ridge magmas: Evidence for assimilation of seawater-influenced components. *Geochimica et Cosmochimica Acta*, *53*(12), 3131–3143. https://doi.org/10.1016/0016-7037(89)90094-X

Miyoshi, M., Sano, T., Shimizu, K., Delacour, A., Hasenaka, T., Mori, Y., & Fukuoka, T. (2015). Boron and chlorine contents of basalts from the Shatsky Rise, IODP Expedition 324: Implications for the alteration of oceanic plateaus. In C. R. Neal, W. W. Sager, T. Sano, & E. Erba (Eds.), *The Origin, Evolution, and Environmental Impact of Oceanic Large Igneous Provinces* (Vol. 511, pp. 69–84).

Pettke, T., Halter, W. E., Webster, J. D., Aigner-Torres, M., & Heinrich, C. A. (2004). Accurate quantification of melt inclusion chemistry by LA-ICPMS: A comparison with EMP and SIMS and advantages and possible limitations of these methods. *Lithos*, *78*(4), 333–361. https://doi.org/10.1016/j.lithos.2004.06.011

Portnyagin, M. V., Ponomareva, V. V., Zelenin, E. A., Bazanova, L. I., Pevzner, M. M., Plechova, A. A., et al. (2020). TephraKam: Geochemical database of glass compositions in tephra and welded tuffs from the Kamchatka volcanic arc (northwestern Pacific). *Earth System Science Data*, *12*(1), 469–486. https://doi.org/10.5194/essd-12-469-2020

Reekie, C. D. J., Jenner, F. E., Smythe, D. J., Hauri, E. H., Bullock, E. S., & Williams, H. M. (2019). Sulfide resorption during crustal ascent and degassing of oceanic plateau basalts. *Nature Communications*, *10*(1), 82. https://doi.org/10.1038/s41467-018-08001-3

Sano, T., Hanyu, T., Tejada, M. L. G., Koppers, A. A. P., Shimizu, S., Miyazaki, T., et al. (2020). Two-stages of plume tail volcanism formed Ojin Rise Seamounts adjoining Shatsky Rise. *Lithos*, *372–373*, 105652. https://doi.org/10.1016/j.lithos.2020.105652

Sano, T., Shimizu, K., Ishikawa, A., Senda, R., Chang, Q., Kimura, J. I., et al. (2012). Variety and origin of magmas on Shatsky Rise, northwest Pacific Ocean. *Geochemistry, Geophysics, Geosystems*, *13*(8). https://doi.org/10.1029/2012GC004235

Shimizu, K., Shimizu, N., Sano, T., Matsubara, N., & Sager, W. (2013). Paleo-elevation and subsidence of ~145Ma Shatsky Rise inferred from CO_2 and H_2O in fresh volcanic glass. *Earth and Planetary Science Letters*, *383*, 37–44. https://doi.org/10.1016/j.epsl.2013.09.023

St. John, K. E. K., & Krissek, L. A. (1999). Regional patterns of Pleistocene ice-rafted debris flux in the North Pacific. *Paleoceanography*, *14*(5), 653–662. https://doi.org/10.1029/1999PA900030

Stroncik, N. A., & Haase, K. M. (2004). Chlorine in oceanic intraplate basalts: Constraints on mantle sources and recycling processes. *Geology*, *32*(11), 945–948. https://doi.org/10.1130/g21027.1

Sun, S.-S., & McDonough, W. F. (1989). Chemical and isotopic systematics of oceanic basalts: Implications for mantle composition and processes. *Geological Society, London, Special Publications*, *42*(1), 313–345. https://doi.org/10.1144/gsl.sp.1989.042.01.19

Tejada, M. L. G., Geldmacher, J., Hauff, F., Heaton, D., Koppers, A. A. P., Garbe-Schönberg, D., et al. (2016). Geochemistry and age of Shatsky, Hess, and Ojin Rise seamounts: Implications for a connection between the Shatsky and Hess Rises. *Geochimica et Cosmochimica Acta*, *185*, 302–327. https://doi.org/10.1016/j.gca.2016.04.006

Wallace, P., & Carmichael, I. S. E. (1992). Sulfur in basaltic magmas. *Geochimica et Cosmochimica Acta*, *56*(5), 1863–1874. https://doi.org/10.1016/0016-7037(92)90316-B

Wallace, P. J., & Edmonds, M. (2011). The sulfur budget in magmas: Evidence from melt inclusions, submarine glasses, and volcanic gas emissions. *Reviews in Mineralogy and Geochemistry*, *73*(1), 215–246. https://doi.org/10.2138/rmg.2011.73.8